Cluster soft excess and SZ effect in the era of high resolution X-ray astronomy

Richard Lieu
Jonathan Mittaz

University of Alabama, Huntsville

XMM-Newton has definitely confirmed the cluster soft excess

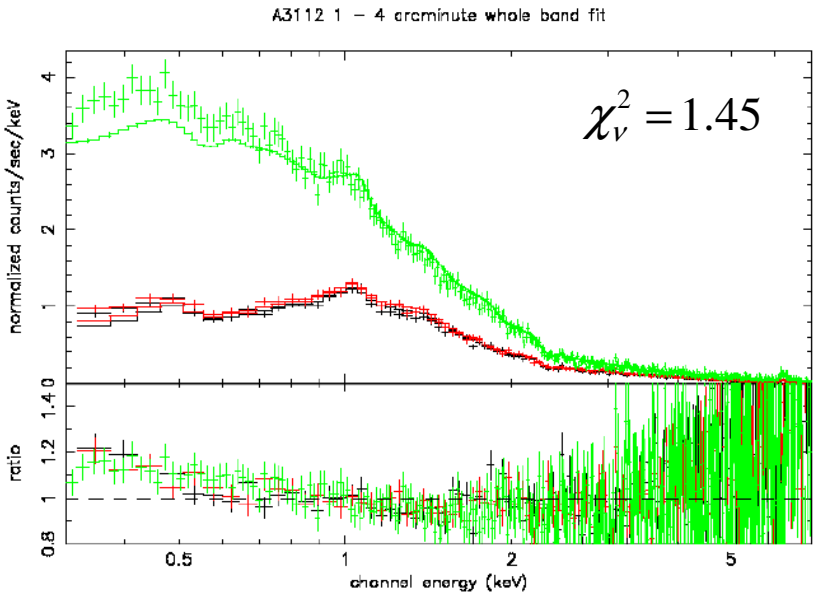

Fit with a single temperature across the whole 0.3-7 keV band shows significant residuals indicating a cluster soft excess

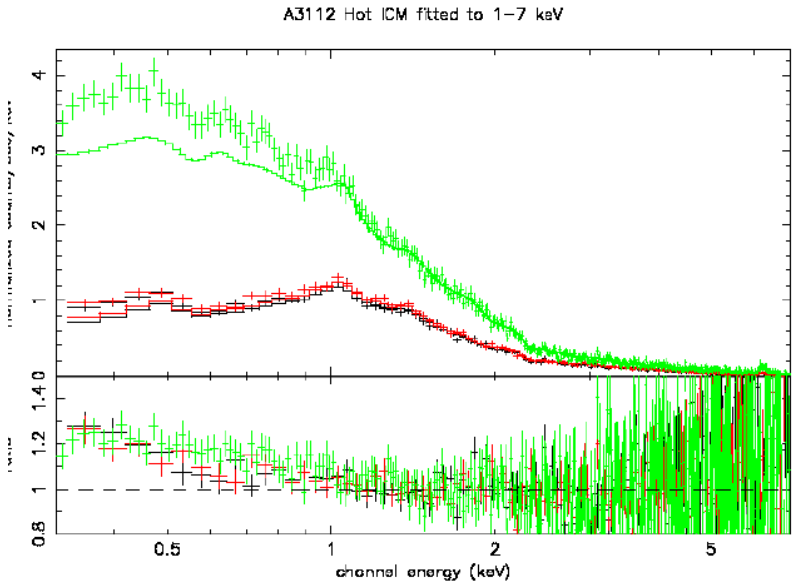

Fit to the hot ICM (1-7 keV) showing the cluster soft excess at energies below 1 keV. The excess is seen at > 20% level above the hot ICM model

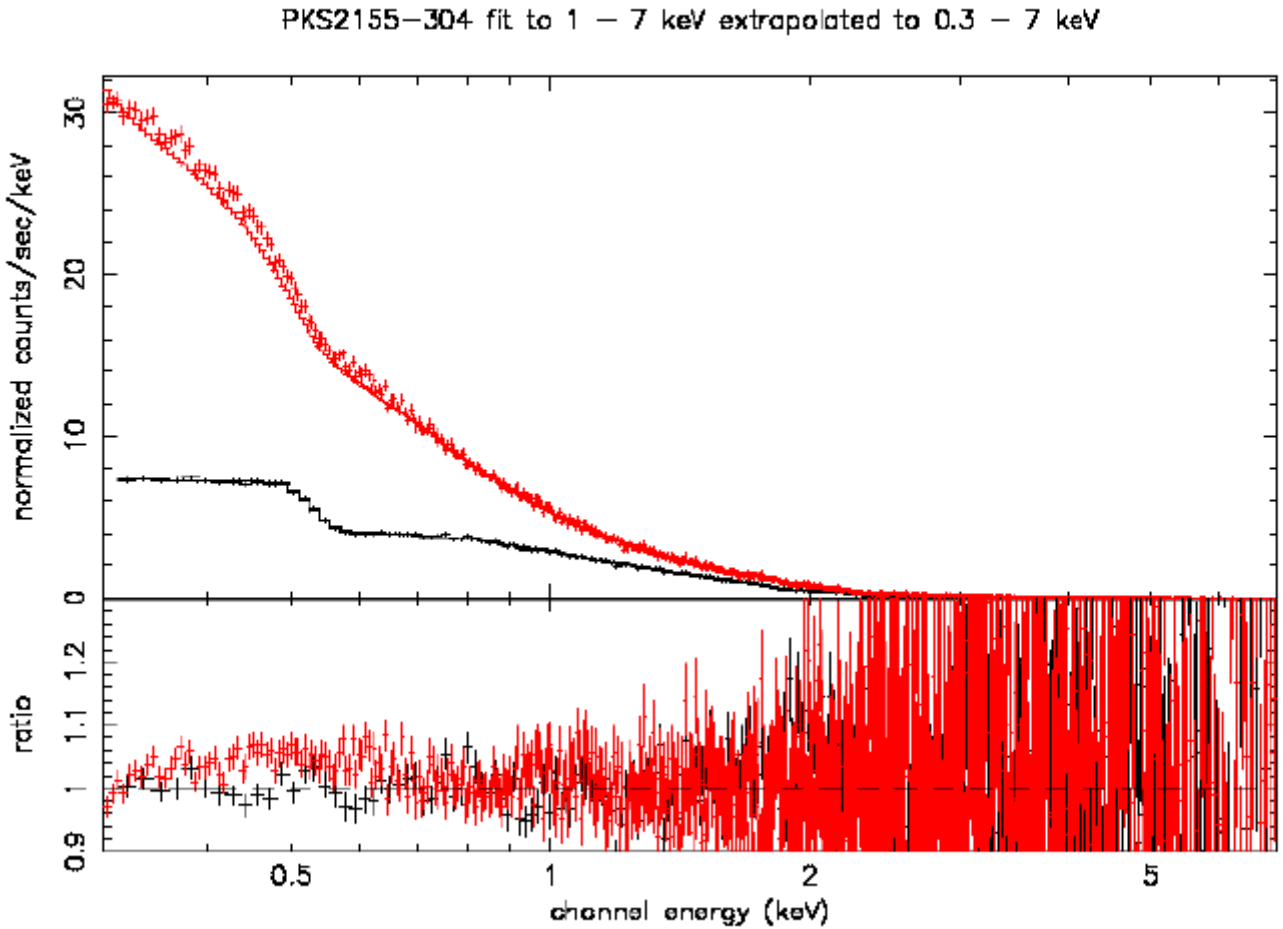

Fit to PKS2155-304 to demonstrate the systematic errors in extrapolating to lower energies from a 1-7 keV fit. Note the maximum residuals are at the 8% level, much less than residuals seen showing the presence of a cluster soft excess

XMM Calibration uncertainties for PM/MOS ~ 5%

Soft excess is above the calibrational uncertainties

Taken from “EPIC status of calibration and data analysis” Kirsch et al. XMM-SOC-CAL-TN-0018

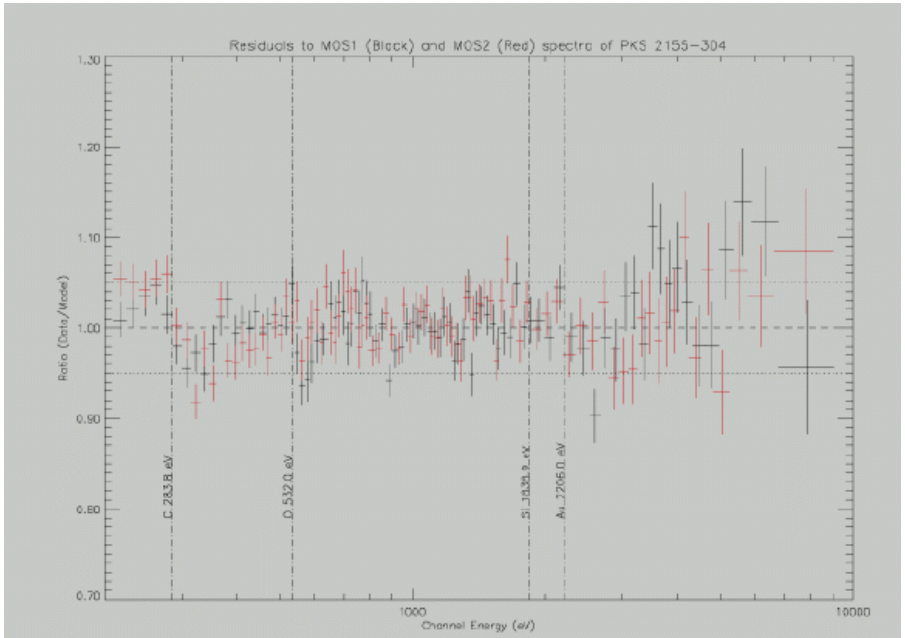

Figure 1-15: MOS PKS2155

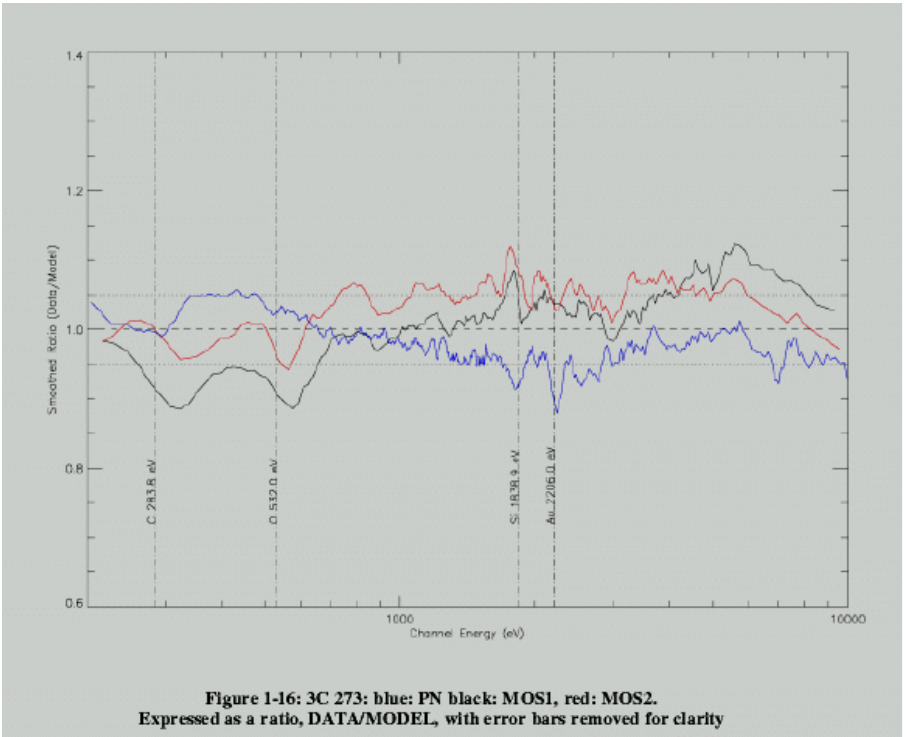

Figure 1-16: 3C 273: blue: PN black: MOS1, red: MOS2.
Expressed as a ratio, DATA/MODEL, with error bars removed for clarity

Note for A3112, cluster soft excess is not a background effect

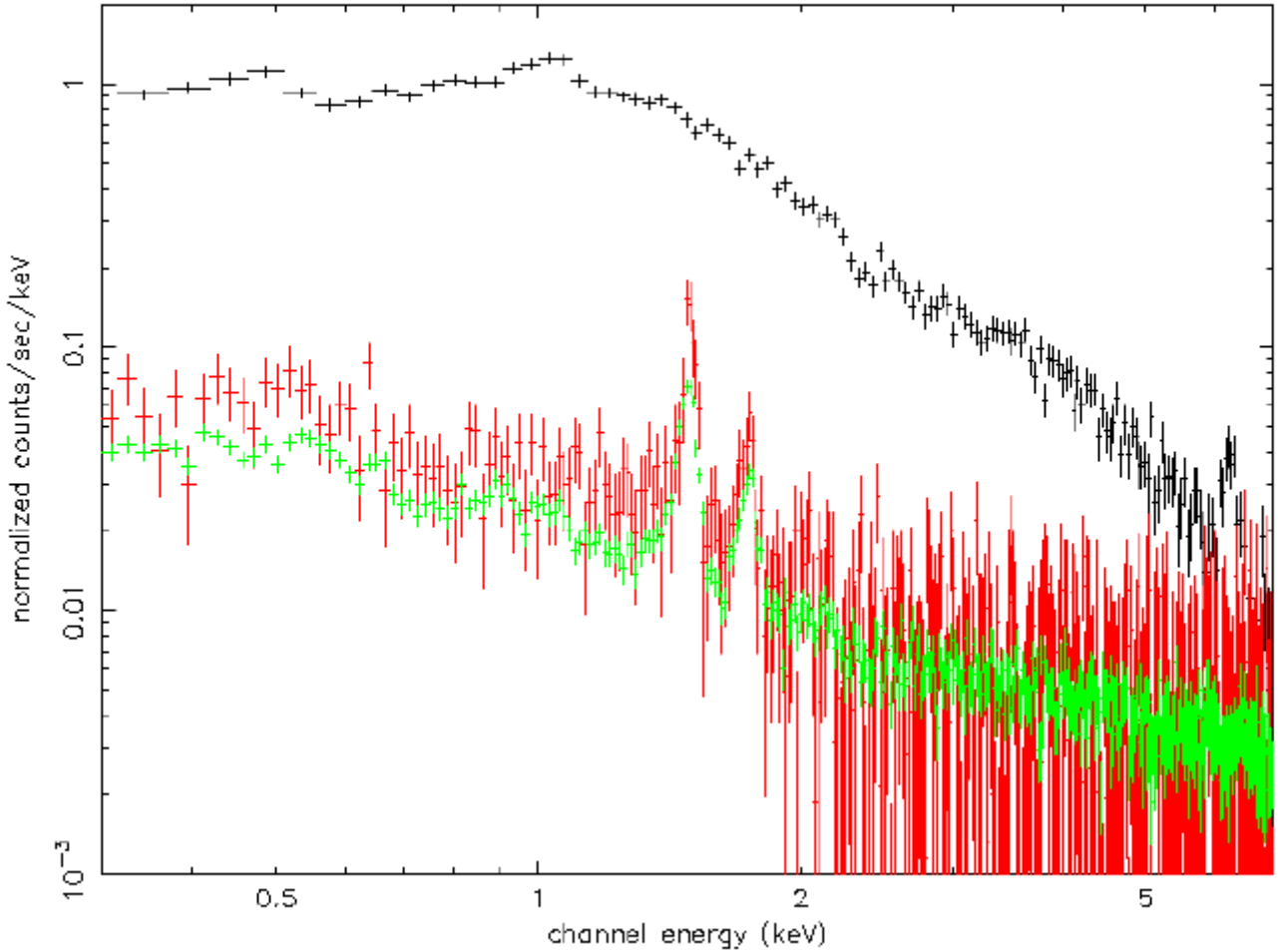

Central soft excess for AS1101 and A3112 ROSAT/XMM joint fits for region from any background subtraction issues

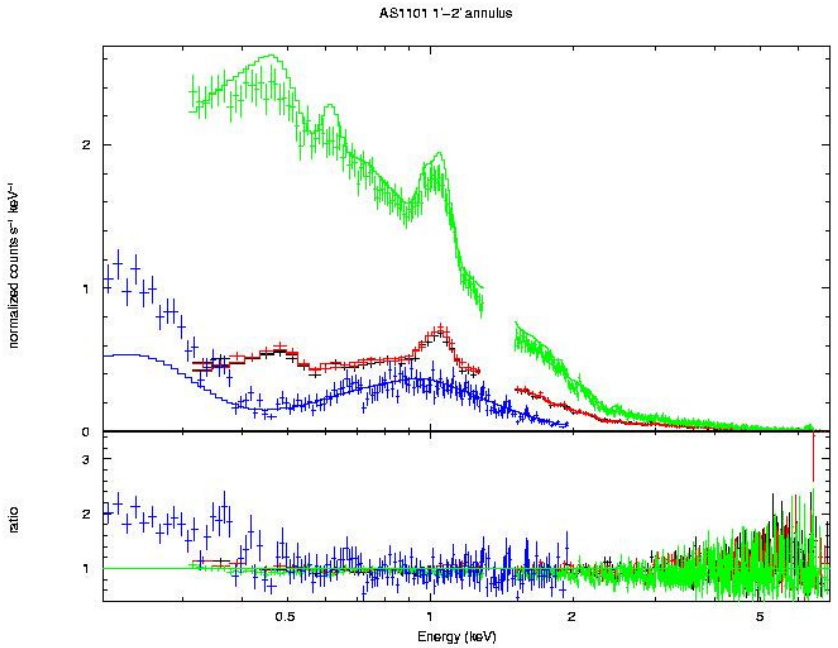

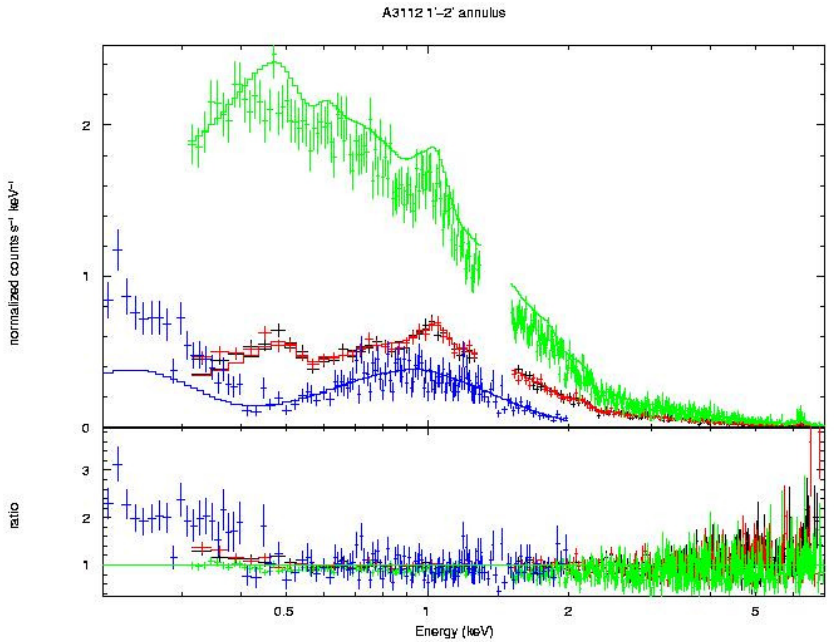

Outer soft excess for AS1101 and A3112

AS1101 4 - 6 arcminute

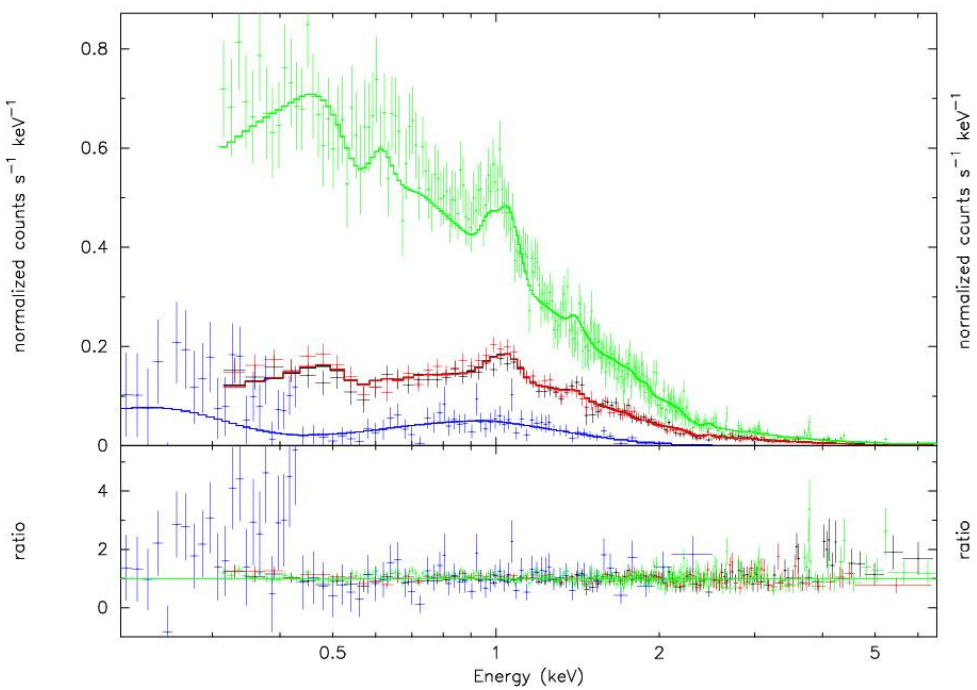

A3112 4 - 6 arcminute

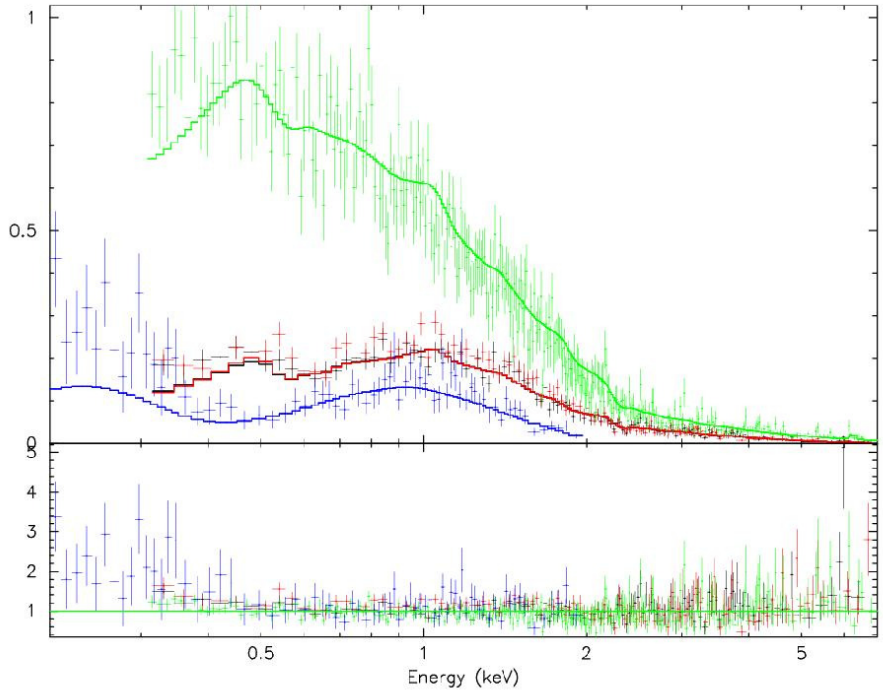

Central soft excess (no background issues) for A1795 and Coma

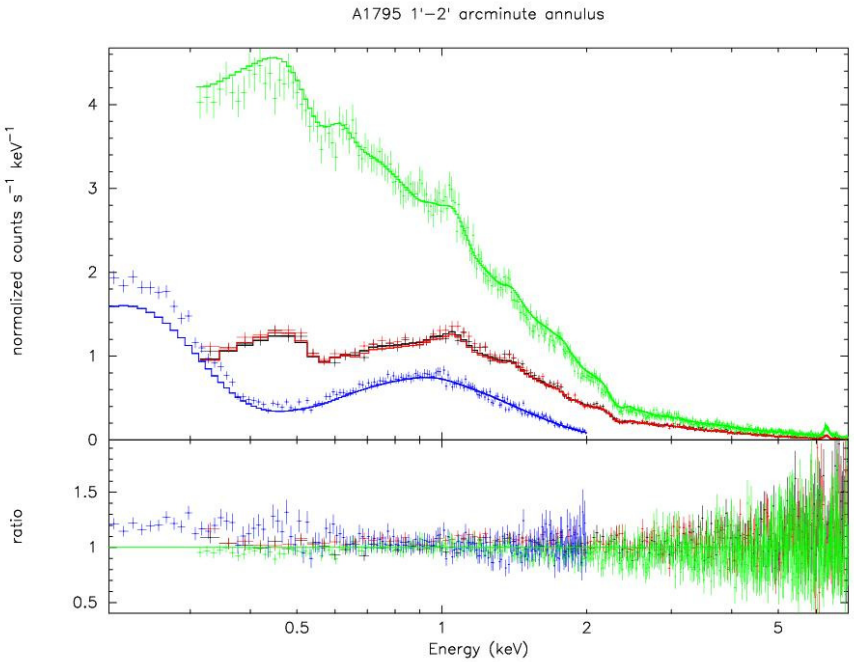

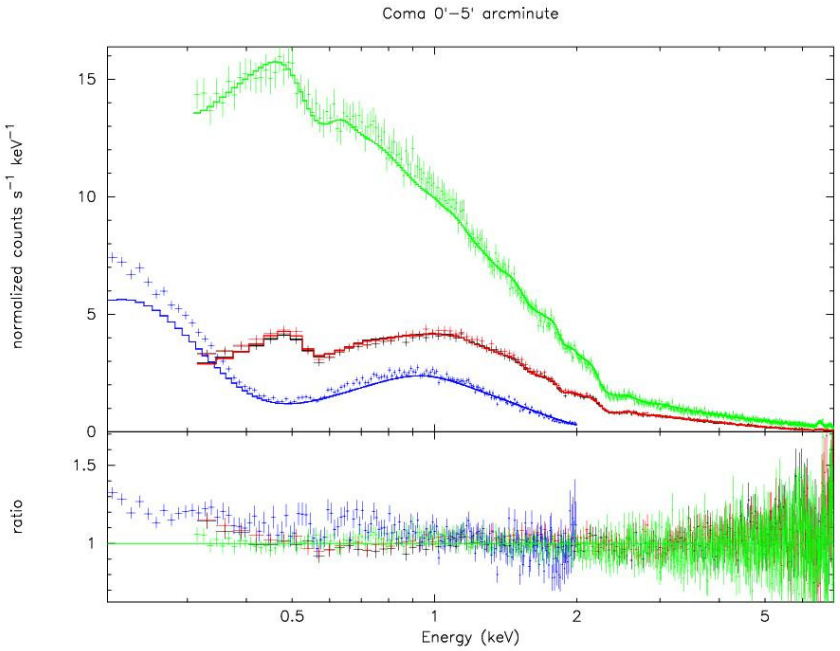

Physical constraints on the model

For intracluster origin of the WHIM

$$P_{warm} = P_{hot} \rightarrow n_w = (n_h / 10^{-3} cm^{-3}) \left(\frac{T_h}{T_w} \right)$$

If we take $T_h = 10 T_w, n_w > 10^{-2} cm^{-3}$

Radiative cooling time is important

$$\tau = 6 \times 10^9 (T / 10^6 K)^{0.5} (n_w / 10^{-3} cm^{-3})^{-1} yrs$$

For $T_w \sim 10^6 K, n_w > 10^{-2} cm^{-3}$ $\tau < 6 \times 10^8 years$

WHAT SUSTAINS THE WARM GAS AGAINST SUCH RAPID RADIATIVE COOLING?

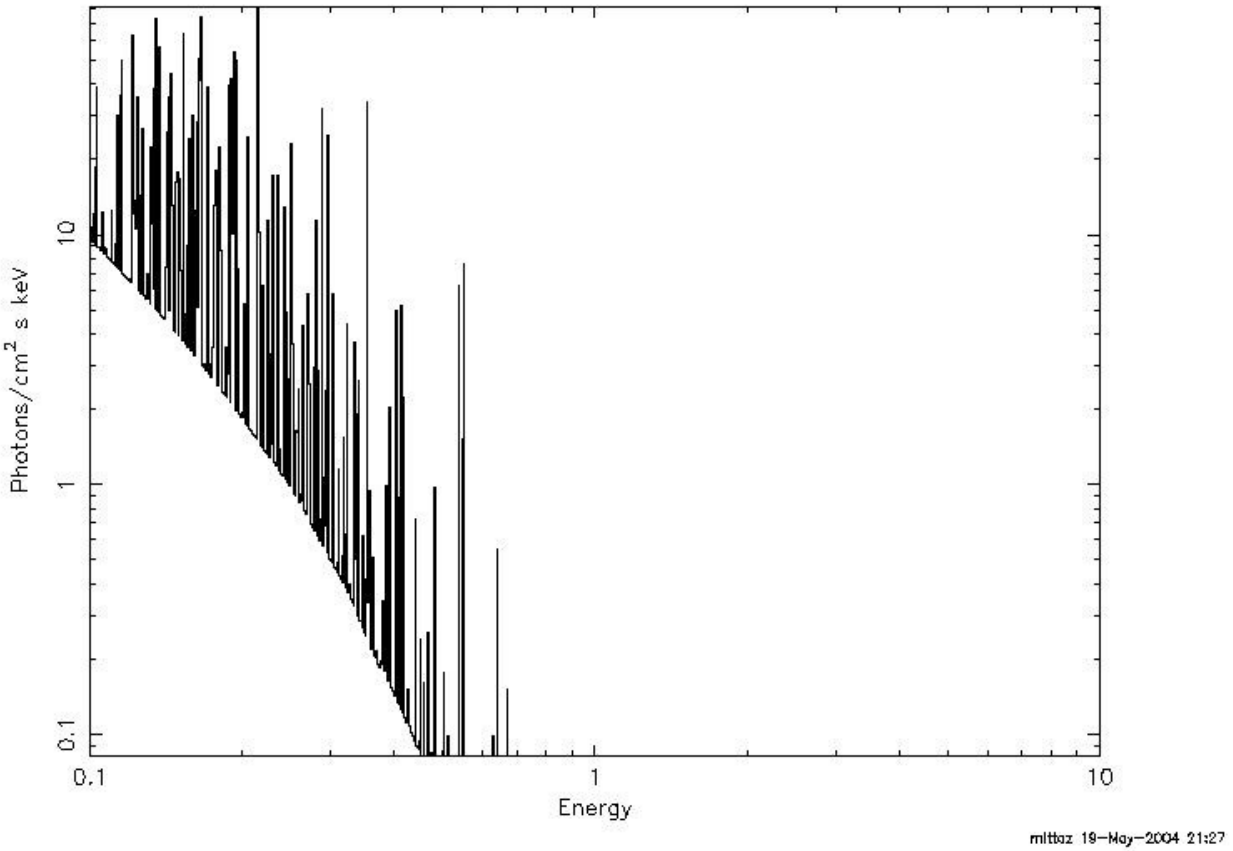

Thermal (mekal) model kT $\approx 10^6\,K$

The discovery of cluster soft excess as extra photon emission in the 0.2 – 0.5 keV range above the level expected from the low energy tail of the virialised intracluster gas at X-ray temperatures was made by the EUVE mission in 1995

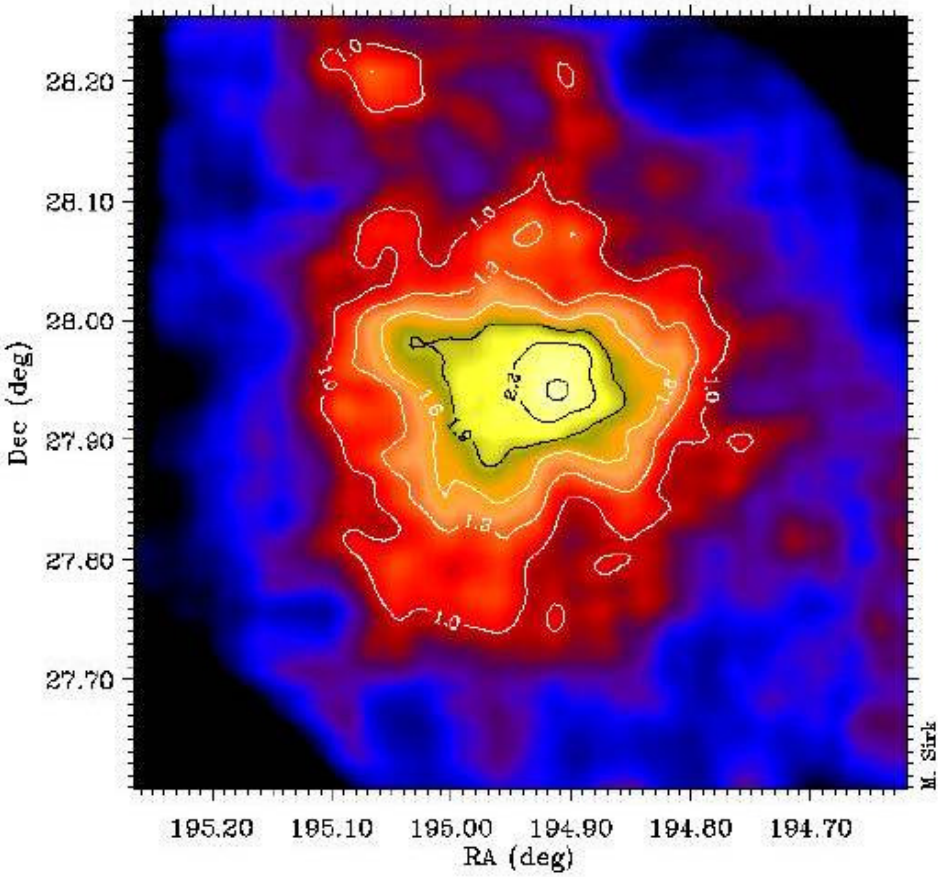

Coma Cluster in the EUV

Giant ¼ keV Halo centered at Coma (as detailed by the ROSAT sky survey)

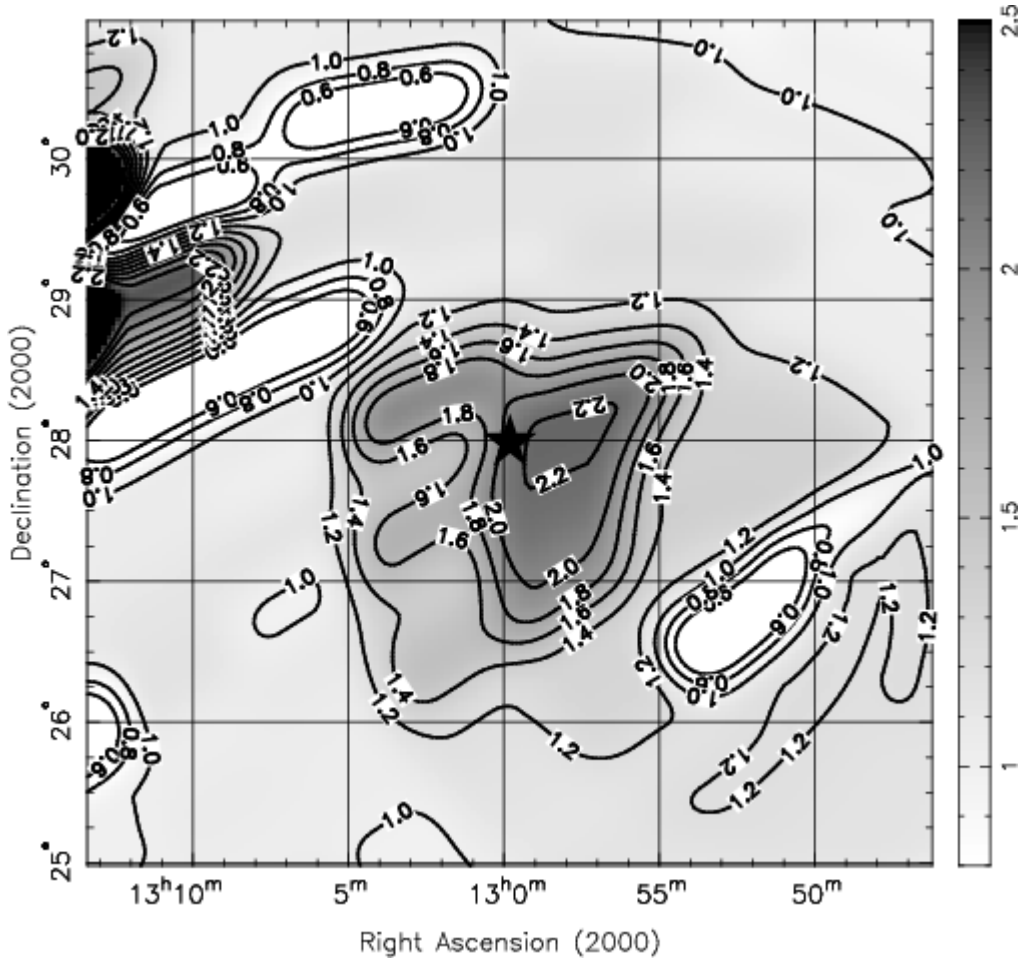

ROSAT/PSPC Radial surface brightness of Coma
(Bonamente, Joy, & Lieu, 2003, ApJ, 585, 722)

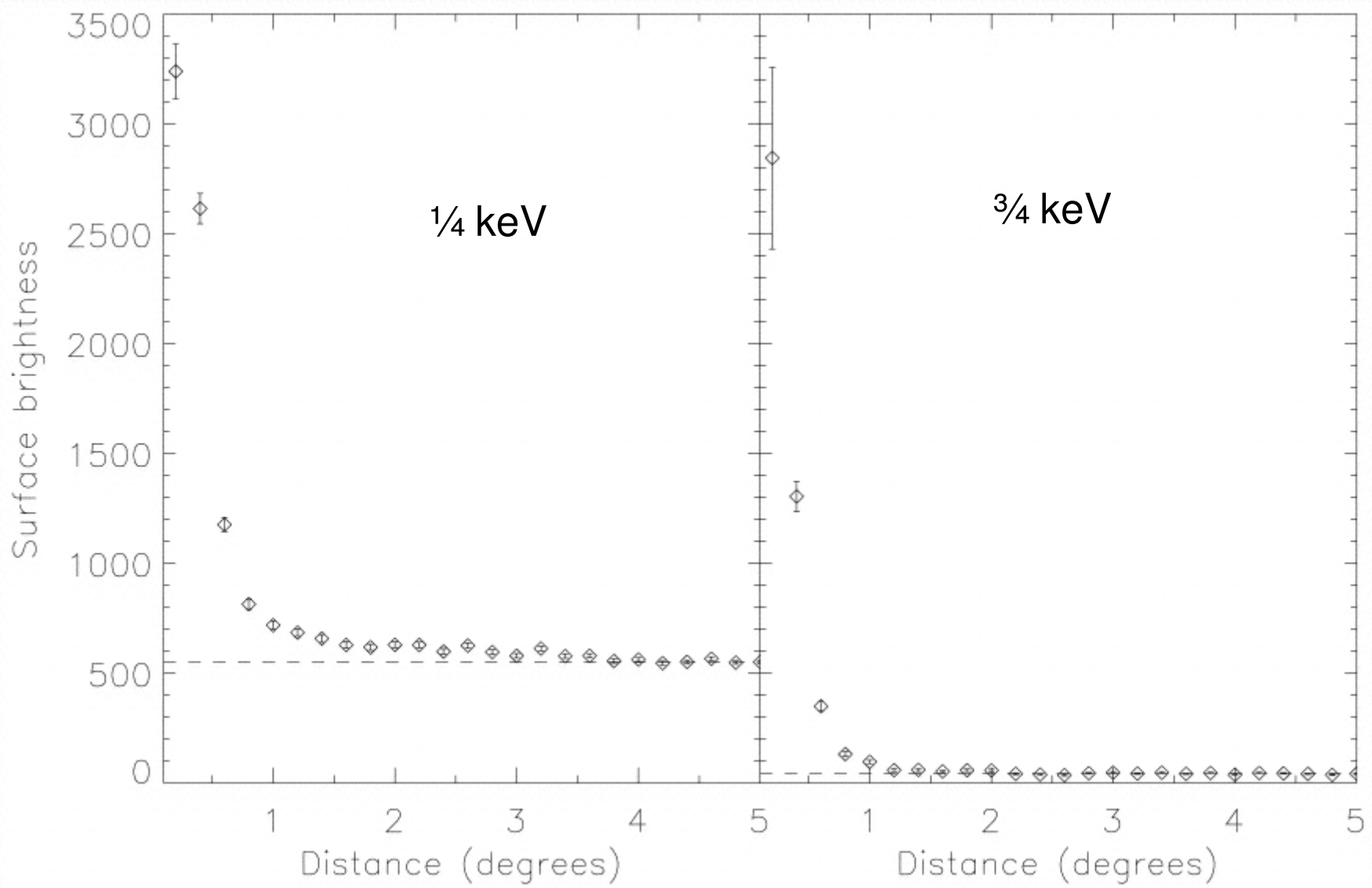

ROSAT/PSPC data of the Coma cluster (50'-70' annulus)

X-ray thermal model (kT~8keV)

Fitting the excess with a 2nd component

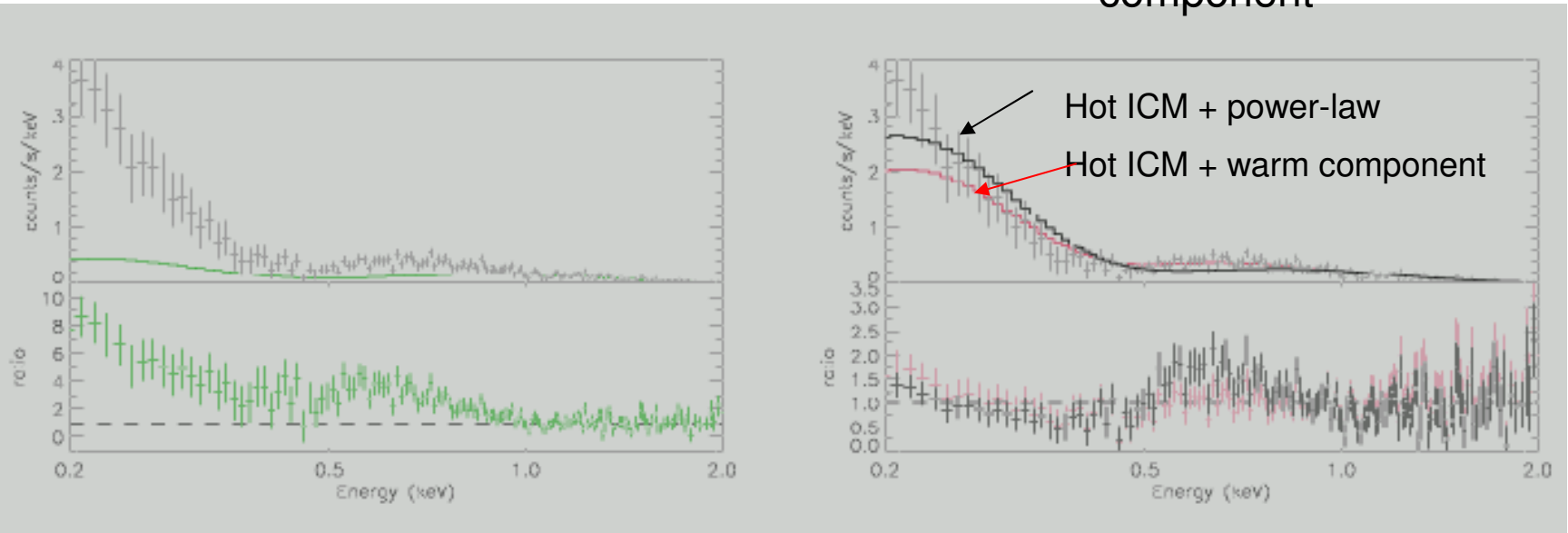

Unlike the cluster core, strong soft excess at the outskirts of Coma. Statistically the thermal model is preferred (to a power law).

The warm gas here may be part of the WHIM (e.g. Cen & Ostriker 1999) not in physical contact with the hot ICM. XMM-Newton confirmation of the Coma soft excess halo.

Coma cluster 0.5 – 2 keV with XMM-Newton pointings

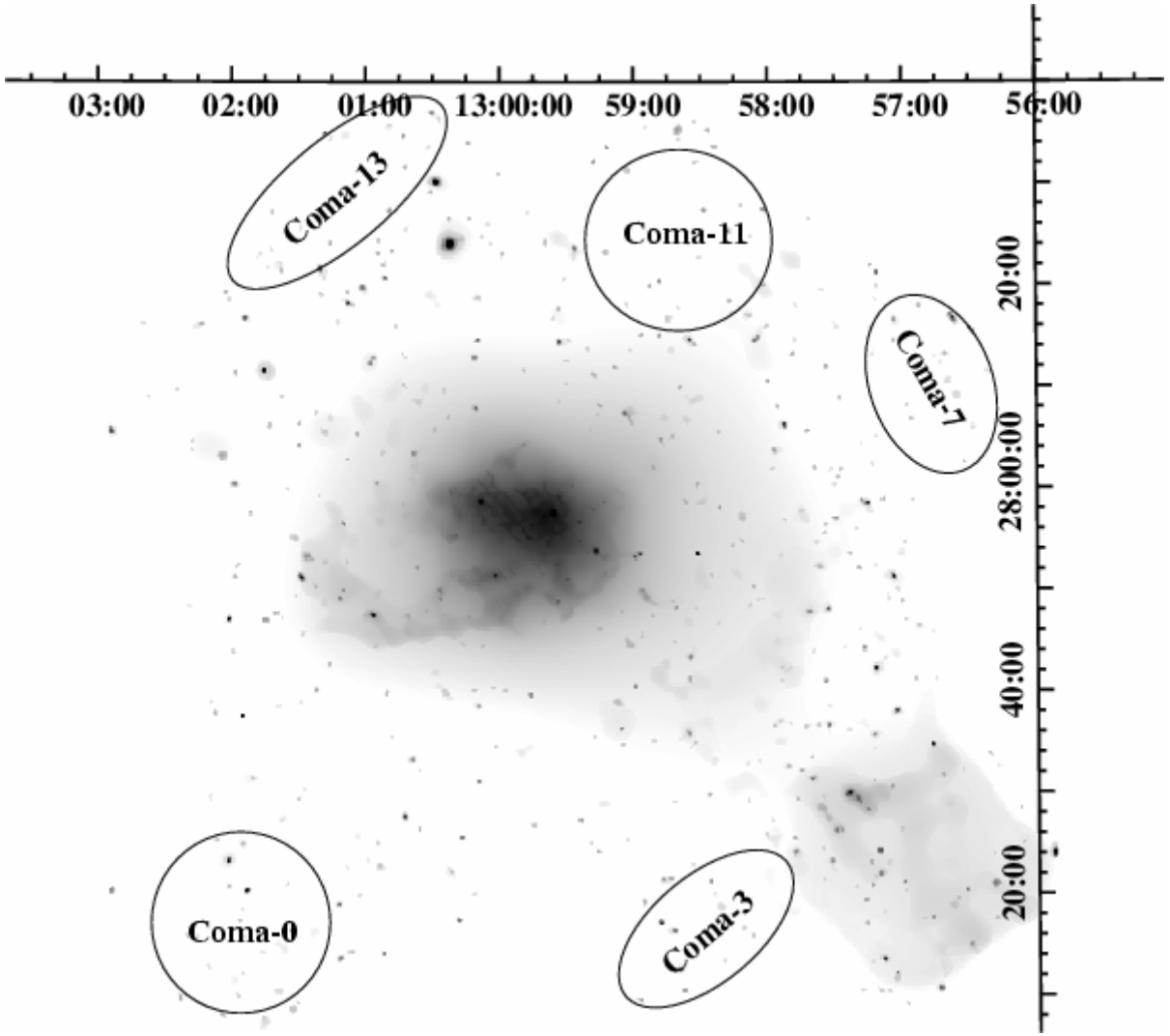

XMM-Newton spectrum of the Coma 11 region
(Finoguenov, Briel & Henry, 2003, A&A, 410, 777)

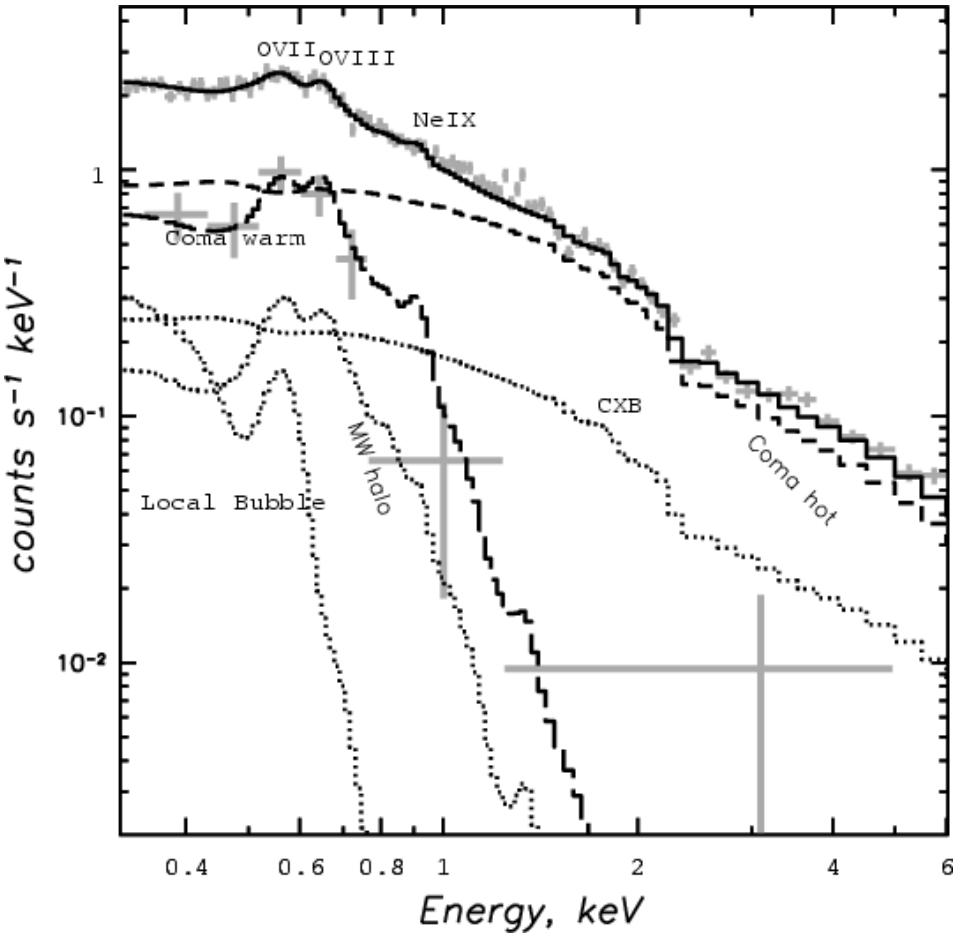

RGS spectra of X-Comae which lies behind the Coma cluster. Shown are the individual spectra from three separate observations of X-Comae together with the position of the OVII line at the redshift of Coma and of the Galaxy. The expected absorption from the CSE cannot be seen

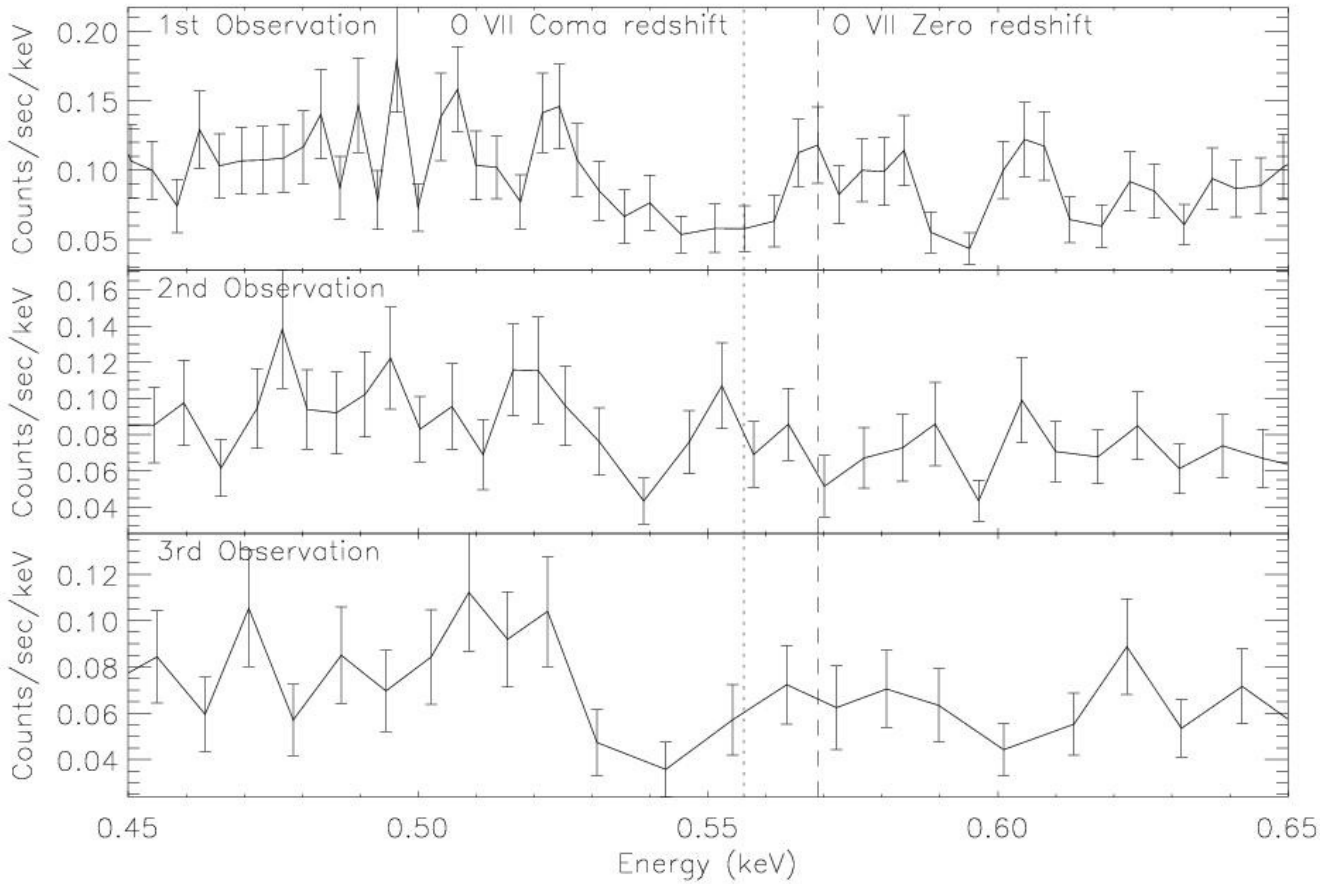

Same as previous slide but now all observations have been added. Again, there is no line at the expected redshift of Coma

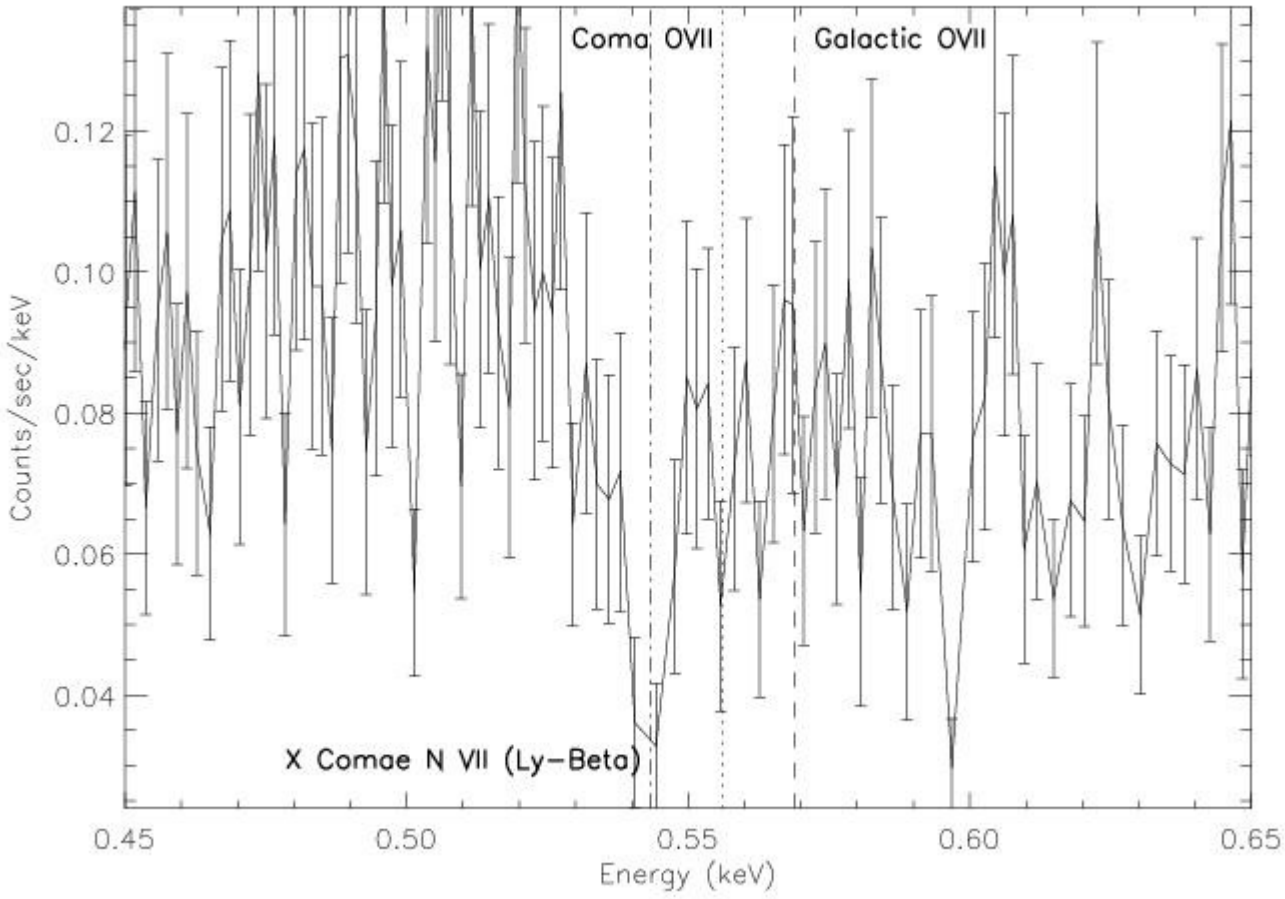

One of the recent claims regarding the soft excess is the detection of OVII line emission

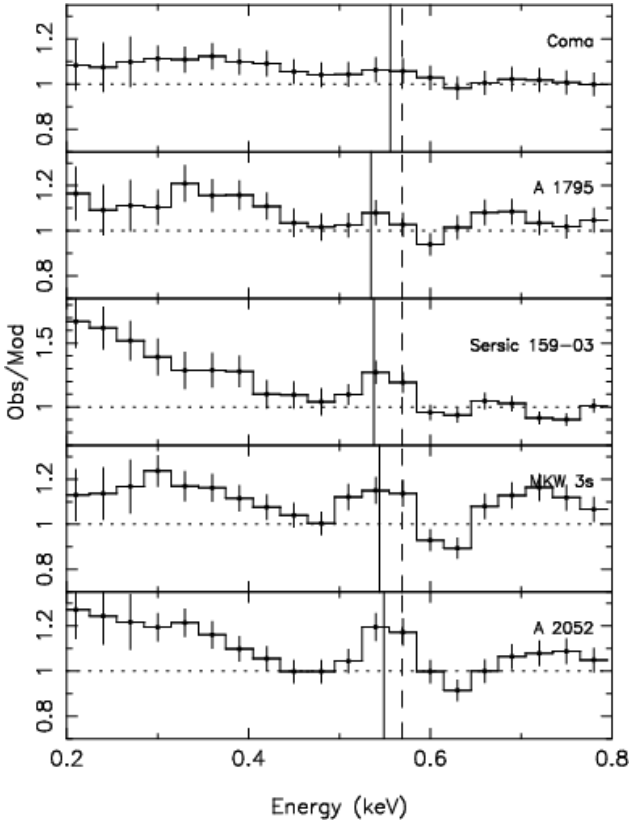

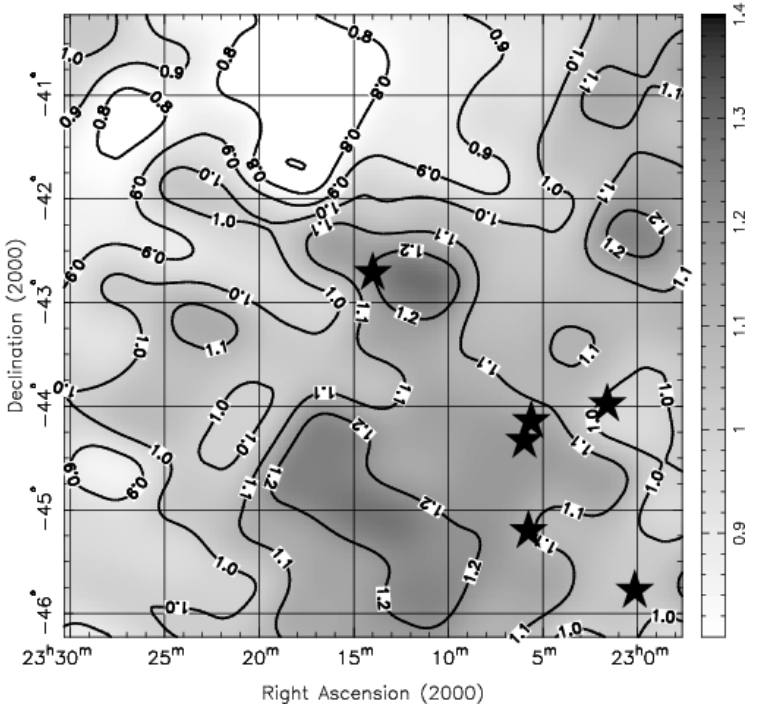

Kaastra et al. (2003)

However, the importance of good background subtraction cannot be overstated – depending on what assumptions you take the potential background can vary by a lot.

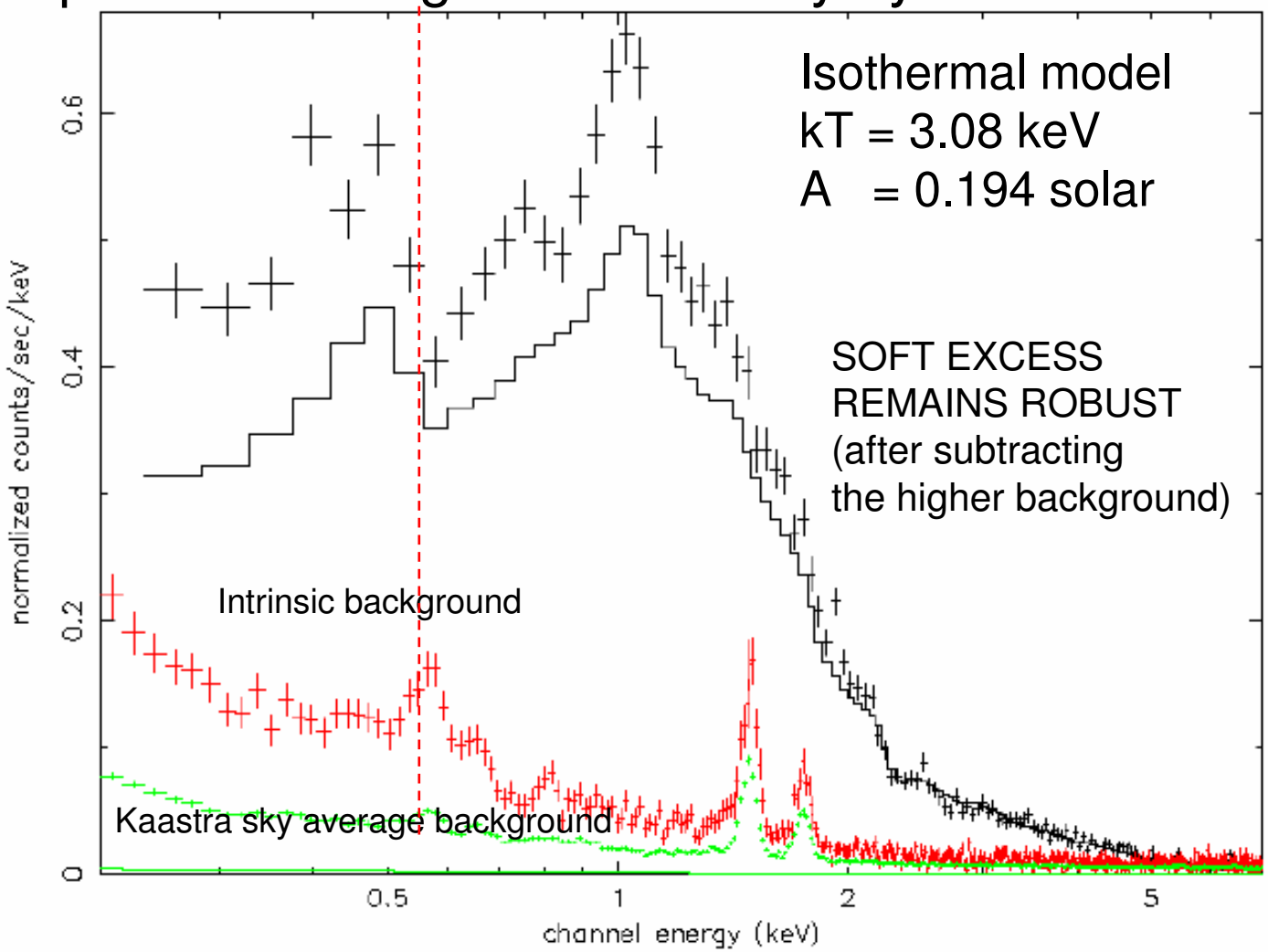

AS1101 (2'-5') with ICM model (fitted from 2-7 keV) and backgrounds

For AS1101 there is also little evidence for redshifted OVII line emission

AS1101 10'-13' background spectrum. OVII+OVIII lines consistent with Galactic emission and not associated with the cluster redshift (z=0.058)

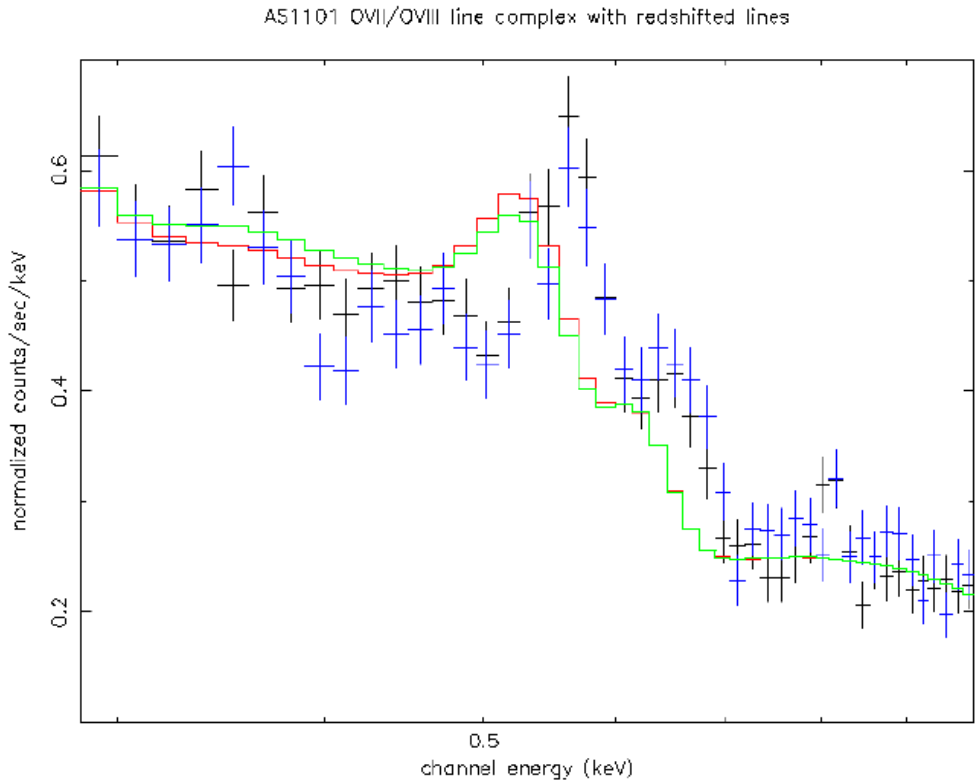

OVII+OVIII lines positioned at the cluster redshift in AS1101 background

Line fit to the OVII+OVIII complex with no constraint on the energy of the line

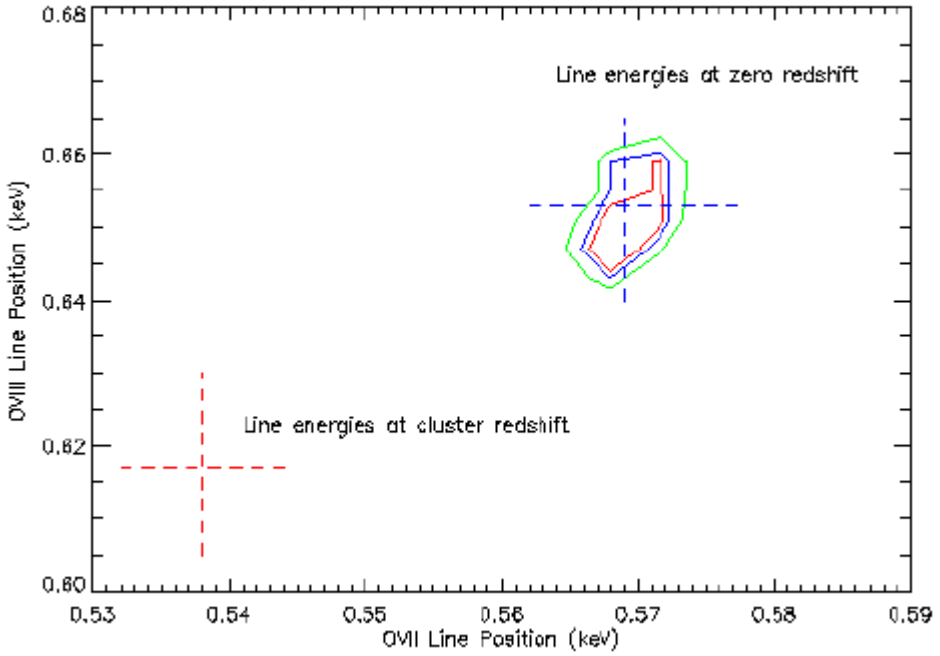

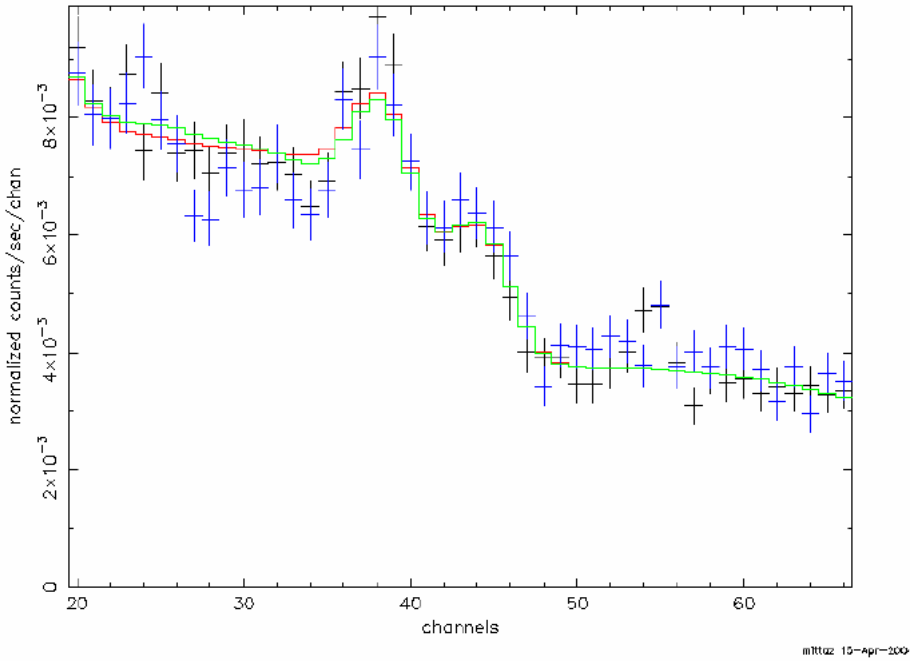

Line completely consistent with zero redshift i.e. Galactic origin

Suzaku observations of A2052 seem to show no need for a strong thermal OVII line from a large scale soft WHIM component

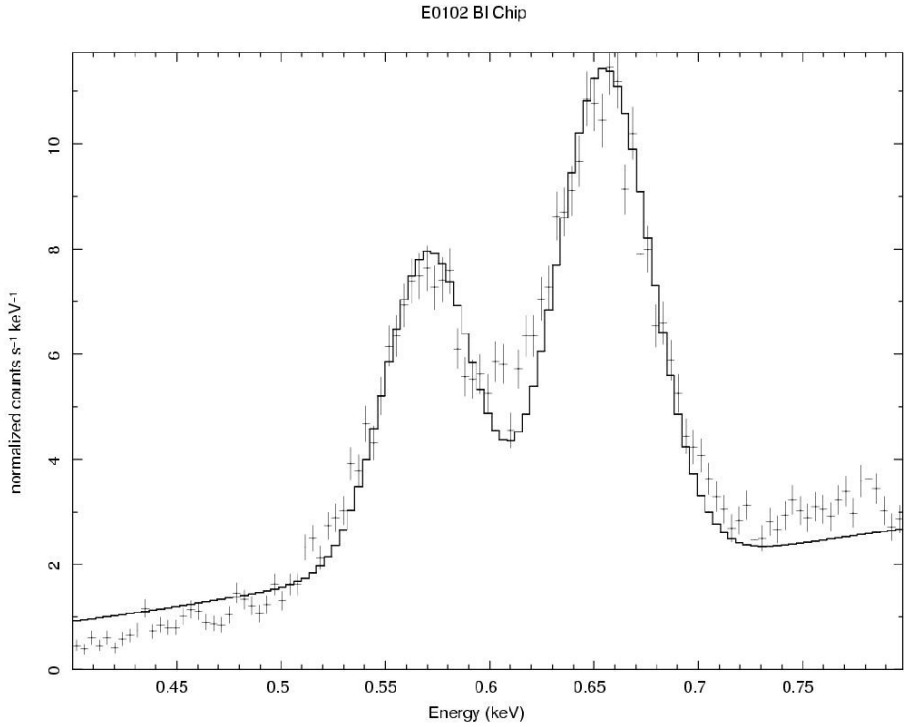

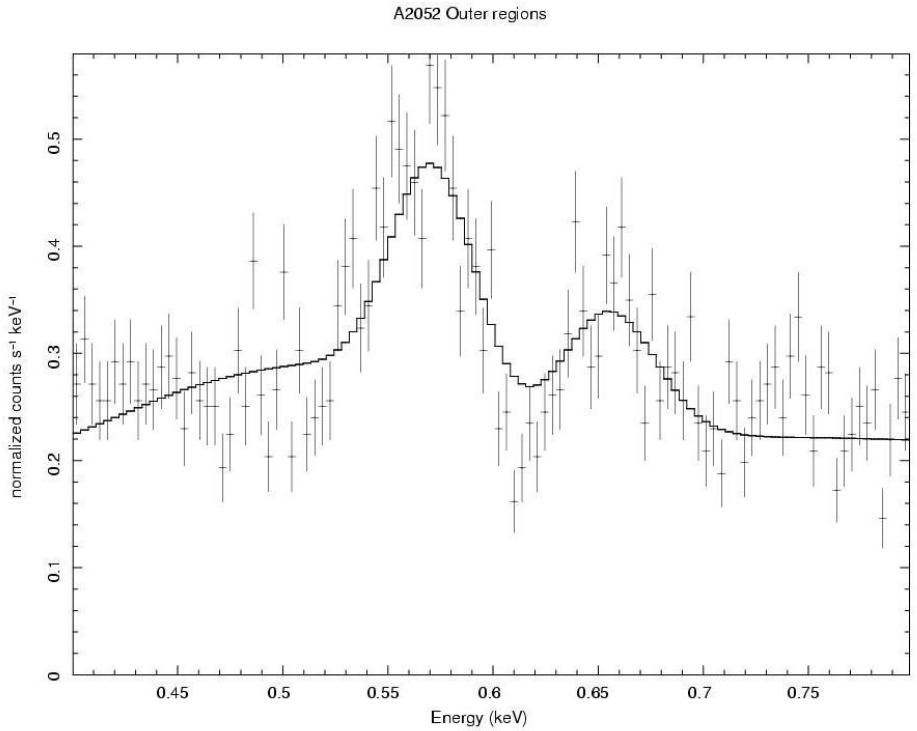

10 ksec Constellation-X calorimeter simulation of the OVII lin region for A2052 where the redshifted OVII line has 10% of the background line flux (~ consistent with Suzaku observation). Redshifted OVII line is clearly seen.

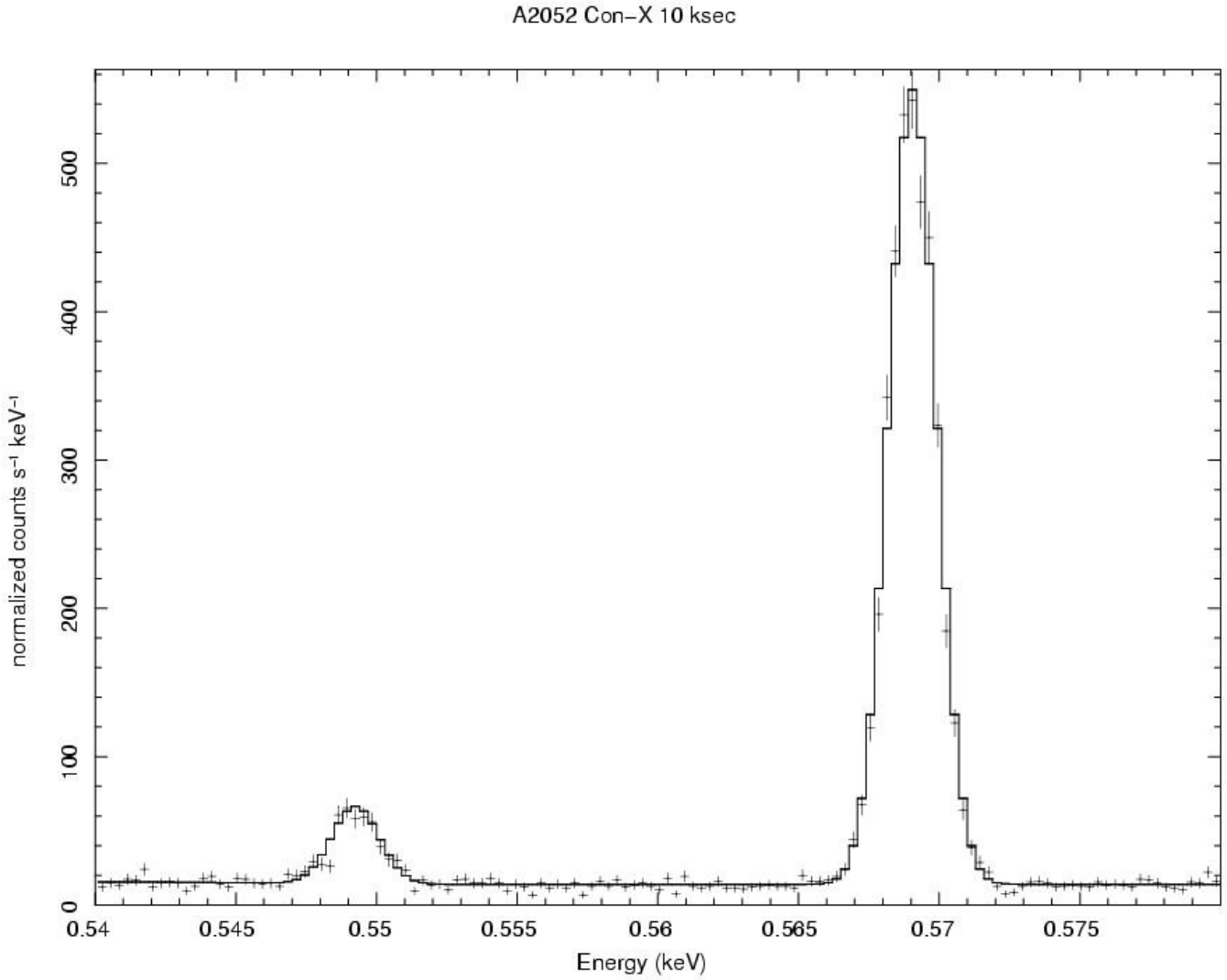

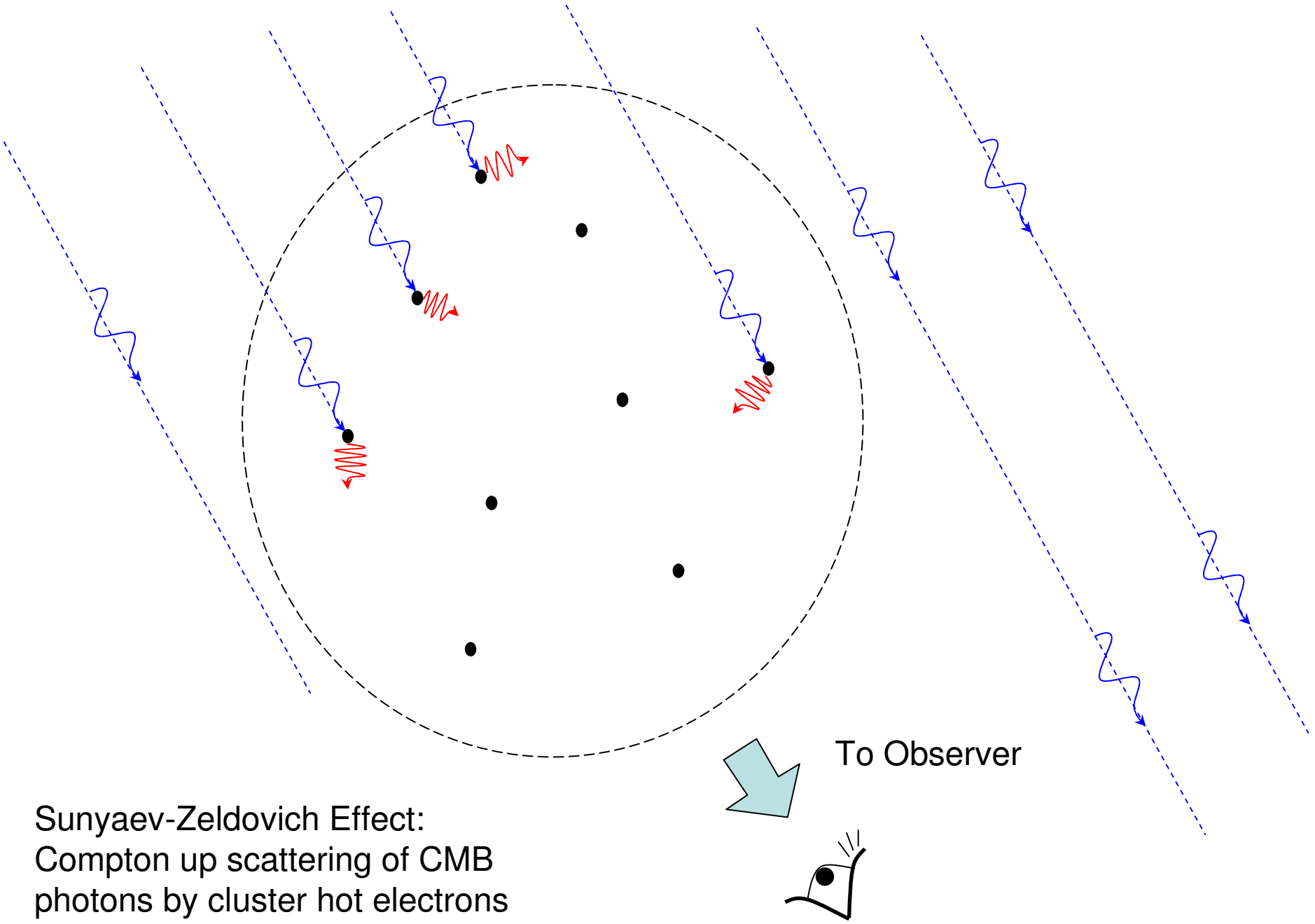

Sunyaev-Zeldovich Effect:
Compton up scattering of CMB
photons by cluster hot electrons

Basics of the Sunyaev-Zeldovich Effect

$$\frac{\Delta T(\theta)}{T_{CMB}} = -\frac{kT}{m_e c^2}\sigma_T \int dl\, n_e \left[\frac{x(e^x+1)}{e^x-1} - 4\right]$$

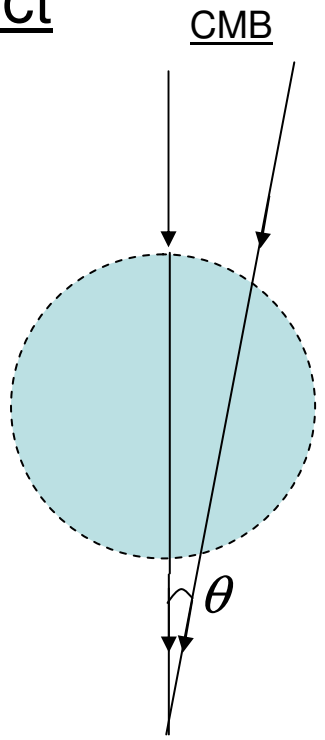

The electron density of the hot gas is obtained by fitting ROSAT X-ray surface brightness profiles $I_X(\theta)$ with the 2 parameter isothermal β -model ignoring the central cooling flow

$$n_e(r) = n_0\left[1+\left(\frac{r}{r_e}\right)^2\right]^{-3\beta/2} \Rightarrow I_X(\theta) \propto n_0^2\left[1+\left(\frac{\theta}{\theta_C}\right)^2\right]^{-3\beta+\frac{1}{2}}$$

The decrement in T_{CMB} is then given by

$$\Delta T_{SZ}(\theta) = \Delta T_{SZ}(0)\left[1+\left(\frac{\theta}{\theta_C}\right)^2\right]^{-\frac{3\beta}{2}+\frac{1}{2}} \quad \text{where } \Delta T_{SZ}(0) = -38.8\mu K\left(\frac{n}{10^{-3}\,cm^{-3}}\right)\left(\frac{kT}{keV}\right)\left(\frac{r_C}{Mpc}\right)\left[\frac{j(x)}{-2}\right]\frac{\Gamma\left(\frac{3\beta}{2}-\frac{1}{2}\right)}{\Gamma\left(\frac{3\beta}{2}\right)}$$

$$\text{with } j(x) = \frac{x(e^x+1)}{e^x-1} - 4$$

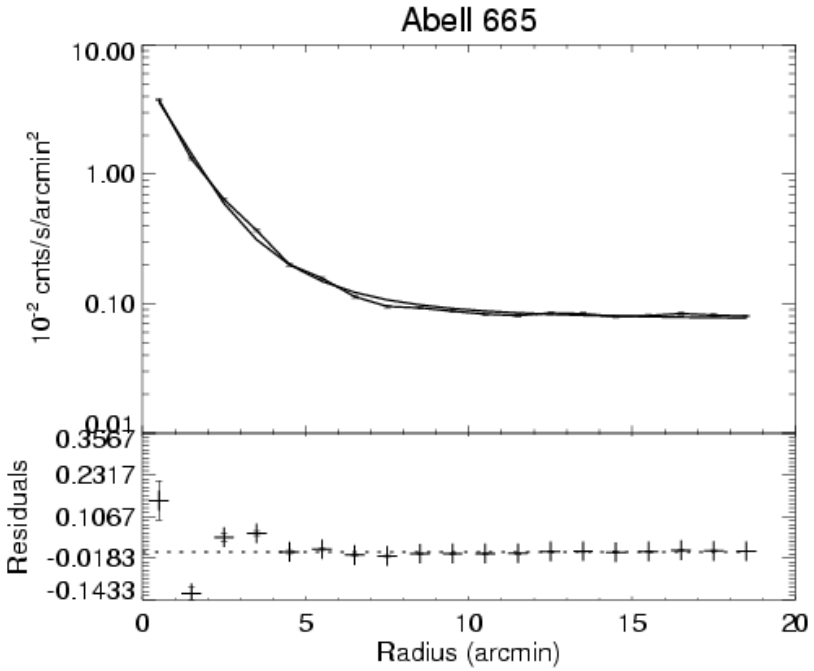
Abell 665
10.00
1.00
0.10
0.01
10^{-2} cnts/s/arcmin^2
0.3567
0.2317
0.1067
-0.0183
-0.1433
Residuals
0
5
10
15
20
Radius (arcmin)

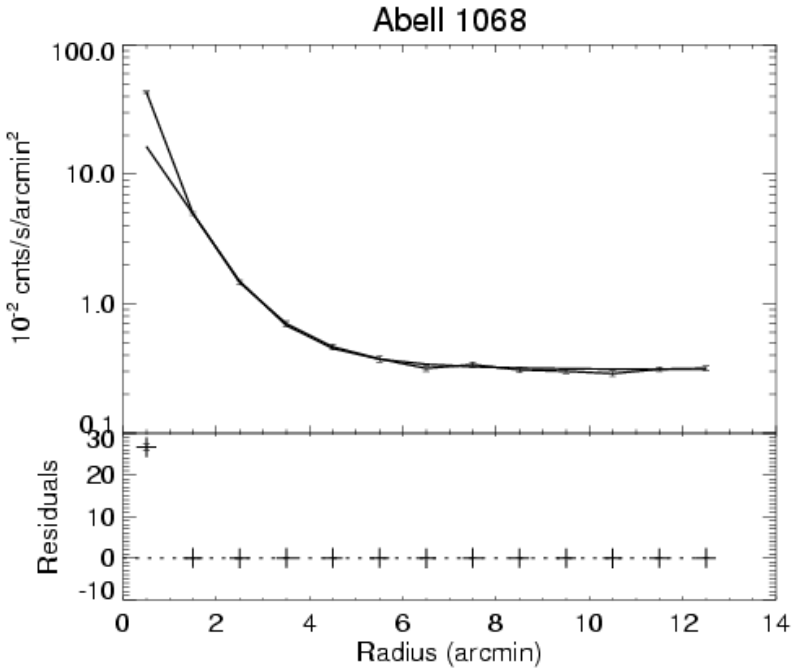
Abell 1068
100.0
10.0
1.0
0.1
10^{-2} cnts/s/arcmin^2
30
20
10
0
-10
Residuals
0
2
4
6
8
10
12
14
Radius (arcmin)

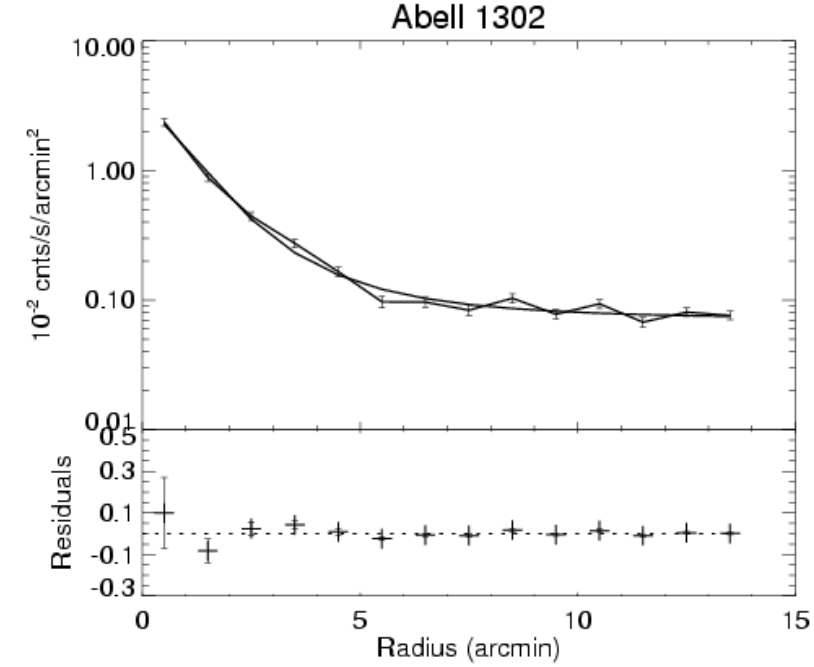
Abell 1302
10.00
1.00
0.10
0.01
10^{-2} cnts/s/arcmin^2
0.5
0.3
0.1
-0.1
-0.3
Residuals
0
5
10
15
Radius (arcmin)

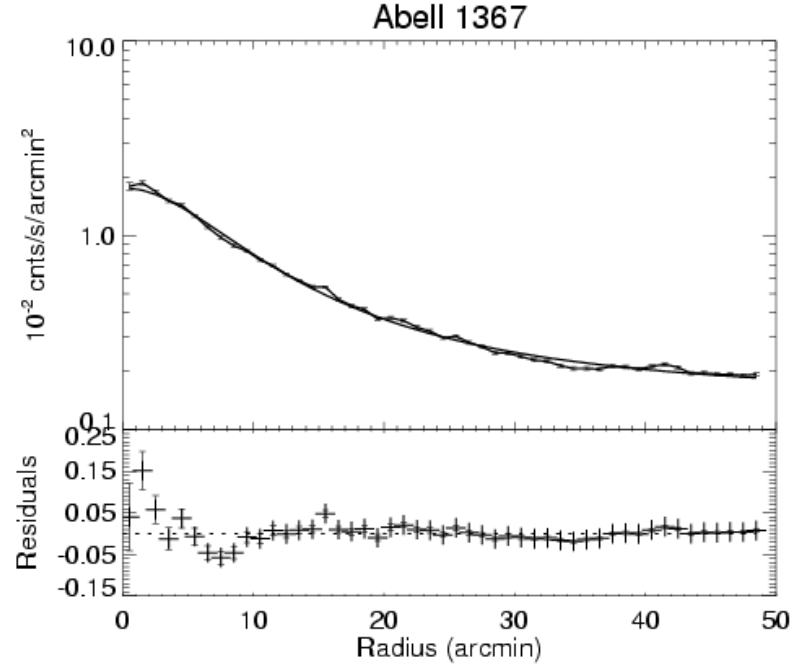
Abell 1367
10.0
1.0
0.1
10^{-2} cnts/s/arcmin^2
0.25
0.15
0.05
-0.05
-0.15
Residuals
0
10
20
30
40
50
Radius (arcmin)

Name	Galactic (2000)		Redshift	kT	n_0	β	R_{core}	$\Delta T0_Q$	$\Delta T0_V$	$\Delta T0_W$
	Long.	Lat.		(keV)	$\times 10^{-3}$ cm^{-3}		(arcmin)	mK	mK	mK
Abell 85	115.053	-72.064	0.055	7.0	$14.64^{+0.33}_{-0.34}$	$0.58^{+0.03}_{-0.03}$	$1.7^{+0.6}_{-0.8}$	$-0.92^{+0.43}_{-0.32}$	$-0.87^{+0.40}_{-0.30}$	$-0.75^{+0.35}_{-0.26}$
Abell 133	149.761	-84.233	0.057	5.0	$2.98^{+0.13}_{-0.11}$	$0.72^{+0.09}_{-0.07}$	$3.4^{+0.8}_{-0.8}$	$-0.19^{+0.05}_{-0.06}$	$-0.18^{+0.05}_{-0.05}$	$-0.16^{+0.04}_{-0.05}$
Abell 665	149.735	34.673	0.1816	7.0	$3.19^{+0.19}_{-0.22}$	$0.64^{+0.10}_{-0.10}$	$1.3^{+0.1}_{-0.1}$	$-0.38^{+0.08}_{-0.14}$	$-0.36^{+0.07}_{-0.13}$	$-0.31^{+0.06}_{-0.11}$
Abell 1068	179.100	60.130	0.139	5.0	$7.80^{+0.46}_{-0.42}$	$0.90^{+0.17}_{-0.13}$	$1.6^{+0.5}_{-0.5}$	$-0.41^{+0.15}_{-0.15}$	$-0.39^{+0.14}_{-0.14}$	$-0.33^{+0.12}_{-0.12}$
Abell 1302	134.668	48.904	0.116	4.8	$2.88^{+0.19}_{-0.15}$	$0.64^{+0.12}_{-0.08}$	$1.4^{+0.4}_{-0.3}$	$-0.17^{+0.05}_{-0.07}$	$-0.16^{+0.05}_{-0.06}$	$-0.14^{+0.04}_{-0.05}$
Abell 1314	151.828	63.567	0.0341	5.0	$1.00^{+0.27}_{-0.26}$	$0.35^{+0.21}_{-0.10}$	$2.6^{+3.2}_{-2.4}$	$-0.44^{+0.58}_{nan}$	$-0.42^{+0.55}_{nan}$	$-0.36^{+0.47}_{nan}$
Abell 1361	153.292	66.581	0.1167	4.0	$2.34^{+nan}_{-0.61}$	$1.79^{+19.04}_{-1.09}$	$5.2^{+43.8}_{-4.2}$	$-0.16^{+0.18}_{nan}$	$-0.15^{+0.17}_{nan}$	$-0.13^{+0.15}_{nan}$
Abell 1367	234.799	73.030	0.0276	3.5	$1.63^{+0.03}_{-0.03}$	$0.52^{+0.02}_{-0.02}$	$8.6^{+0.5}_{-0.6}$	$-0.16^{+0.02}_{-0.02}$	$-0.15^{+0.02}_{-0.02}$	$-0.13^{+0.01}_{-0.02}$
Abell 1413	226.182	76.787	0.143	6.0	$13.65^{+0.77}_{-0.92}$	$0.68^{+0.11}_{-0.11}$	$1.1^{+0.1}_{-0.1}$	$-0.90^{+0.17}_{-0.29}$	$-0.85^{+0.16}_{-0.27}$	$-0.73^{+0.14}_{-0.24}$
Abell 1689	313.387	61.097	0.181	7.0	$13.79^{+0.75}_{-0.89}$	$0.75^{+0.12}_{-0.12}$	$1.0^{+0.0}_{-0.0}$	$-1.00^{+0.17}_{-0.27}$	$-0.94^{+0.16}_{-0.26}$	$-0.81^{+0.14}_{-0.22}$
Abell 1795	33.788	77.155	0.061	7.0	$3.05^{+0.04}_{-0.06}$	$0.99^{+0.04}_{-0.06}$	$5.2^{+0.3}_{-0.4}$	$-0.33^{+0.03}_{-0.03}$	$-0.32^{+0.03}_{-0.03}$	$-0.27^{+0.02}_{-0.02}$
Abell 1914	67.196	67.453	0.171	9.0	$11.21^{+0.19}_{-0.17}$	$0.85^{+0.04}_{-0.04}$	$1.4^{+0.1}_{-0.1}$	$-1.23^{+0.10}_{-0.10}$	$-1.17^{+0.09}_{-0.10}$	$-1.01^{+0.08}_{-0.09}$
Abell 1991	22.762	60.497	0.0586	4.0	$3.14^{+0.56}_{-0.34}$	$0.82^{+0.54}_{-0.22}$	$2.8^{+2.8}_{-8.4}$	$-0.12^{+0.36}_{-0.13}$	$-0.11^{+0.34}_{-0.13}$	$-0.10^{+0.30}_{-0.11}$
Abell 2029	6.505	50.547	0.0767	9.0	$12.07^{+0.19}_{-0.82}$	$0.67^{+0.03}_{-0.11}$	$1.9^{+0.3}_{-0.3}$	$-1.13^{+0.20}_{-0.40}$	$-1.07^{+0.19}_{-0.37}$	$-0.92^{+0.16}_{-0.32}$
Abell 2142	44.213	48.701	0.09	9.0	$7.17^{+0.41}_{-0.49}$	$0.67^{+0.11}_{-0.11}$	$2.3^{+0.2}_{-0.2}$	$-0.97^{+0.20}_{-0.33}$	$-0.92^{+0.19}_{-0.31}$	$-0.79^{+0.16}_{-0.27}$
Abell 2199	62.897	43.697	0.0302	4.5	$7.35^{+0.11}_{-0.19}$	$0.64^{+0.02}_{-0.04}$	$2.8^{+0.7}_{-1.8}$	$-0.23^{+0.15}_{-0.06}$	$-0.22^{+0.14}_{-0.06}$	$-0.19^{+0.12}_{-0.05}$
Abell 2218	97.745	38.124	0.171	6.0	$2.73^{+0.04}_{-0.18}$	$0.72^{+0.03}_{-0.12}$	$1.5^{+0.1}_{-0.1}$	$-0.25^{+0.02}_{-0.07}$	$-0.24^{+0.02}_{-0.07}$	$-0.20^{+0.02}_{-0.06}$
Abell 2219	72.597	41.472	0.228	7.0	$5.32^{+0.12}_{-0.11}$	$0.78^{+0.05}_{-0.04}$	$1.8^{+0.2}_{-0.1}$	$-0.77^{+0.08}_{-0.09}$	$-0.72^{+0.08}_{-0.08}$	$-0.63^{+0.07}_{-0.07}$
Abell 2241	54.784	36.643	0.0635	3.1	$10.94^{+0.45}_{-0.41}$	$0.74^{+0.09}_{-0.07}$	$1.0^{+0.2}_{-0.2}$	$-0.14^{+0.03}_{-0.03}$	$-0.13^{+0.03}_{-0.03}$	$-0.12^{+0.02}_{-0.03}$
Abell 2255	93.975	34.948	0.08	7.0	$2.25^{+0.05}_{-0.04}$	$0.76^{+0.04}_{-0.04}$	$4.6^{+0.4}_{-0.3}$	$-0.36^{+0.03}_{-0.04}$	$-0.34^{+0.03}_{-0.04}$	$-0.29^{+0.03}_{-0.03}$
Abell 2256	111.096	31.738	0.06	7.0	$3.70^{+0.19}_{-0.23}$	$0.85^{+0.14}_{-0.14}$	$5.5^{+0.9}_{-0.9}$	$-0.48^{+0.10}_{-0.13}$	$-0.45^{+0.10}_{-0.13}$	$-0.39^{+0.09}_{-0.11}$
Abell 2597	65.363	-64.836	0.085	4.0	$14.58^{+0.52}_{-0.68}$	$0.71^{+0.07}_{-0.08}$	$1.4^{+0.6}_{-3.3}$	$-0.45^{+1.10}_{-0.21}$	$-0.43^{+1.04}_{-0.20}$	$-0.37^{+0.90}_{-0.17}$
Abell 2670	81.318	-68.516	0.076	3.0	$3.88^{+0.16}_{-0.16}$	$0.64^{+0.07}_{-0.06}$	$1.9^{+0.7}_{-0.8}$	$-0.13^{+0.06}_{-0.05}$	$-0.12^{+0.05}_{-0.05}$	$-0.11^{+0.05}_{-0.04}$
Abell 2717	349.076	-76.390	0.049	3.0	$8.89^{+0.20}_{-0.18}$	$0.64^{+0.04}_{-0.03}$	$1.5^{+0.2}_{-0.1}$	$-0.16^{+0.02}_{-0.02}$	$-0.15^{+0.02}_{-0.02}$	$-0.13^{+0.02}_{-0.02}$
Abell 2744	8.898	-81.241	0.308	11.0	$3.13^{+0.23}_{-0.17}$	$1.60^{+0.44}_{-0.27}$	$3.3^{+0.6}_{-0.4}$	$-0.87^{+0.19}_{-0.22}$	$-0.82^{+0.18}_{-0.21}$	$-0.71^{+0.15}_{-0.18}$
Abell 3301	242.415	-37.409	0.054	7.0	$4.20^{+0.19}_{-0.18}$	$0.49^{+0.05}_{-0.04}$	$1.8^{+0.5}_{-0.4}$	$-0.38^{+0.11}_{-0.14}$	$-0.36^{+0.10}_{-0.14}$	$-0.31^{+0.09}_{-0.12}$
Abell 3558	311.978	30.738	0.048	5.0	$2.58^{+0.04}_{-0.04}$	$0.78^{+0.04}_{-0.03}$	$5.9^{+0.4}_{-0.4}$	$-0.23^{+0.02}_{-0.02}$	$-0.22^{+0.02}_{-0.02}$	$-0.19^{+0.02}_{-0.02}$
Abell 3560	312.578	28.890	0.04	2.0	$4.62^{+0.22}_{-0.20}$	$0.49^{+0.05}_{-0.04}$	$2.6^{+0.6}_{-0.5}$	$-0.12^{+0.03}_{-0.05}$	$-0.12^{+0.03}_{-0.04}$	$-0.10^{+0.03}_{-0.04}$
Abell 3562	313.308	30.349	0.04	4.5	$6.85^{+0.48}_{-0.60}$	$0.47^{+0.08}_{-0.08}$	$1.3^{+0.1}_{-0.1}$	$-0.25^{+0.08}_{-0.24}$	$-0.23^{+0.07}_{-0.23}$	$-0.20^{+0.06}_{-0.20}$
Abell 3571	316.317	28.545	0.04	7.0	$11.92^{+0.29}_{-0.29}$	$0.65^{+0.04}_{-0.04}$	$3.6^{+0.7}_{-0.8}$	$-0.97^{+0.22}_{-0.21}$	$-0.91^{+0.21}_{-0.20}$	$-0.79^{+0.18}_{-0.17}$
Abell 4059	356.833	-76.061	0.046	4.5	$4.95^{+0.42}_{-0.35}$	$1.00^{+0.29}_{-0.19}$	$6.1^{+2.1}_{-1.8}$	$-0.31^{+0.11}_{-0.13}$	$-0.29^{+0.10}_{-0.12}$	$-0.25^{+0.09}_{-0.11}$
Coma	58.080	87.958	0.023	8.2	$4.38^{+0.24}_{-0.29}$	$0.71^{+0.11}_{-0.11}$	$9.8^{+1.6}_{-1.6}$	$-0.59^{+0.14}_{-0.20}$	$-0.56^{+0.13}_{-0.18}$	$-0.48^{+0.11}_{-0.16}$

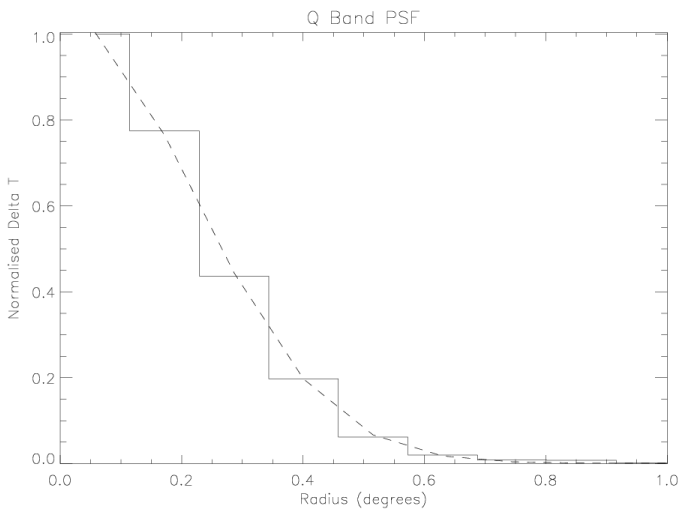
Q Band PSF
Normalised Delta T
Radius (degrees)
0.0
0.2
0.4
0.6
0.8
1.0

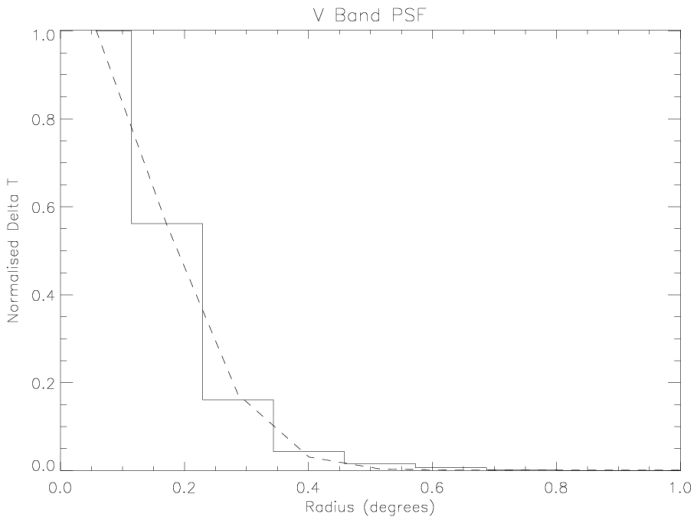
V Band PSF
Normalised Delta T
Radius (degrees)
0.0
0.2
0.4
0.6
0.8
1.0

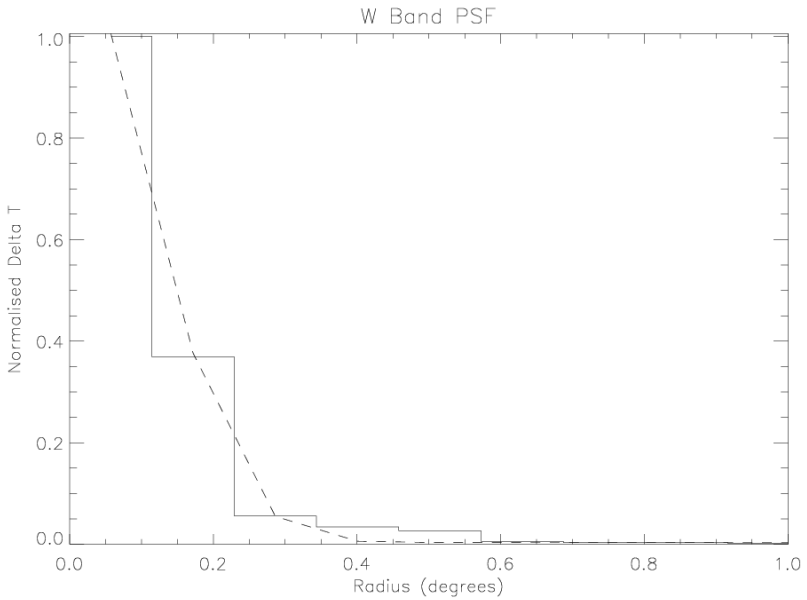
W Band PSF
Normalised Delta T
Radius (degrees)
0.0
0.2
0.4
0.6
0.8
1.0

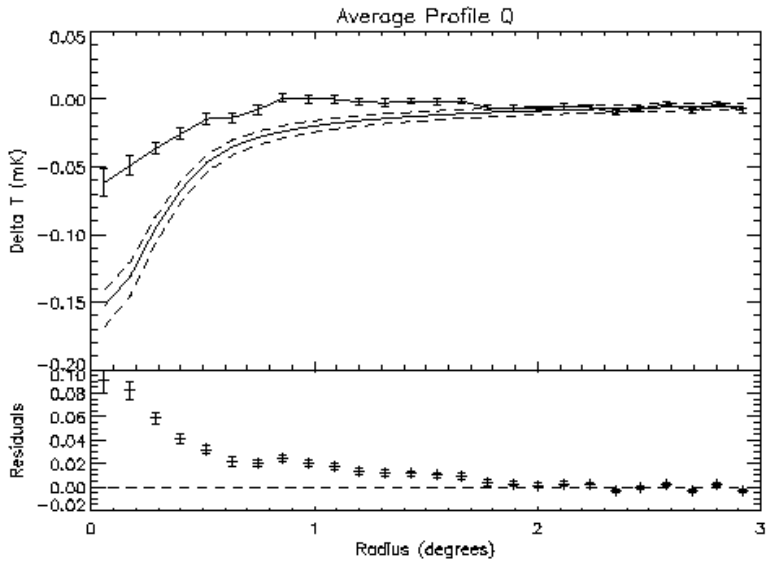
Average Profile Q
Delta T (mK)
Residuals
Radius (degrees)

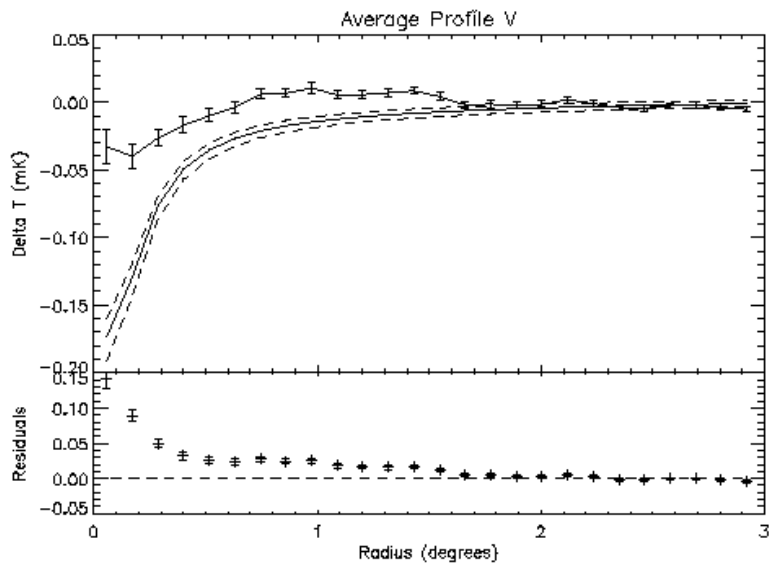
Average Profile V
Delta T (mK)
Residuals
Radius (degrees)

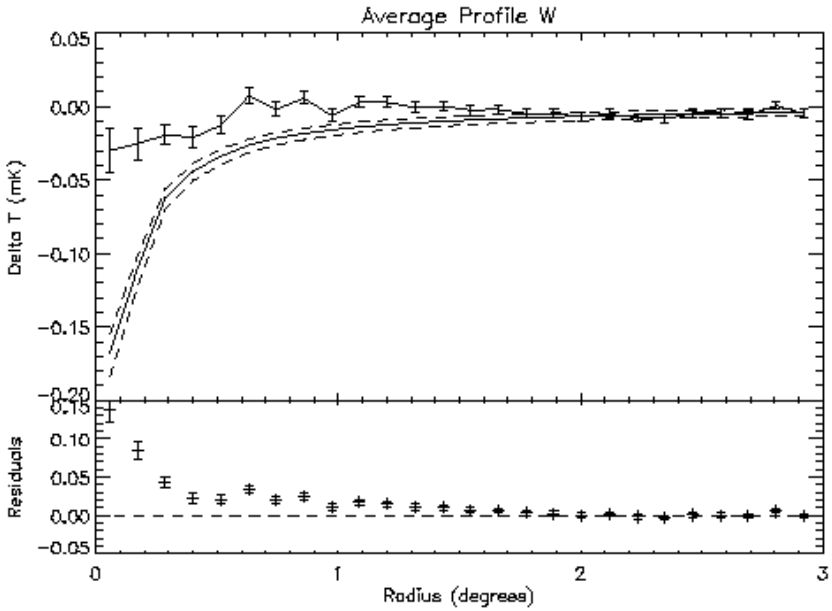
Average Profile W
Delta T (mK)
Residuals
Radius (degrees)

The role of relativistic electrons

- Quenby & Lieu (2006) invoked a power-law population of intracluster relativistic electrons extending to TeV energies.
- In the 0.1-0.5 GeV range they inverse-Compton scatter the CMB to cause soft X-ray excess in clusters.
- At 50 GeV energies synchrotron radiation in micro-gauss field occurs at 40 GHz to reduce the SZE.
- The numbers can account for our observations without violating the EGRET gamma-ray limit.
- The relativistic electrons could be the product of extended intracluster Fermi acceleration, or neutralino annihilation and decay.

Conclusion

- Origin of cluster soft excess is a major puzzle of large scale structures and cosmology.
- Related question is the apparent lack of cluster SZ effect.
- Superior spectral resolution and spatial resolution of Con-X will thrust X-ray astronomy into the era of cosmology through its ability to answer these Q's.